O[superscript 6]-Methylguanine DNA lesions induce an intra-S-phase arrest from which cells exit into apoptosis governed by early and late multi-pathway signaling network activation

Published in final edited form as:
Integr Biol (Camb). 2012 October ; 4(10): 1237–1255. doi:10.1039/c2ib20091k.

O^6-Methylguanine DNA lesions induce an intra-S-phase arrest from which cells exit into apoptosis governed by early and late multi-pathway signaling network activation

Ericka M. Noonan, **Dharini Shah**, **Michael B. Yaffe**, **Douglas A. Lauffenburger**, and **Leona D. Samson**[#]
Biological Engineering Department, Biology Department, Center for Environmental Health Sciences, Koch Institute for Integrative Cancer Research, Massachusetts Institute of Technology, 77 Massachusetts Avenue, Cambridge, MA 02139, USA

Abstract

The *O*^{6}-methylguanine (*O*^{6}MeG) DNA lesion is well known for its mutagenic, carcinogenic, and cytotoxic properties, and understanding how a cell processes such damage is of critical importance for improving current cancer therapy. Here we use human cells differing only in their *O*^{6}MeG DNA methyltransferase (MGMT) or mismatch repair (MMR) status to explore the *O*^{6}MeG/MMR-dependent molecular and cellular responses to treatment with the methylating agent N-methyl-N'-nitro-N-nitrosoguanidine (MNNG). We find that *O*^{6}MeG triggers MMR-dependent cell cycle perturbations in both the first and second cell cycle post treatment. At lower levels of damage, we show that a transient arrest in the second S-phase precedes survival and progression into subsequent cell cycles. However, at higher levels of damage, arrest in the second S-phase coincides with a cessation of DNA replication followed by initiation of apoptotic cell death. Further, we show that entry into apoptotic cell death is specifically from S-phase of the second cell cycle. Finally, we demonstrate the key role of an *O*^{6}MeG/MMR-dependent multi-pathway, multi-time-scale signaling network activation, led by early ATM, H2AX, CHK1, and p53 phosphorylation and followed by greatly amplified late phosphorylation of the early pathway nodes along with activation of the CHK2 kinase and the stress-activated JNK kinase.

INTRODUCTION

Our DNA is constantly under attack by DNA damaging agents that are present not only in our environment but are also formed endogenously during normal cellular metabolism.[1] If not repaired, DNA damage can lead to permanent genetic alterations such as mutations and chromosomal aberrations that ultimately increase our risk of cancer and other diseases.[2] In order to maintain genomic integrity, cells activate a DNA damage response that serves to slow down cell cycle progression so that repair of DNA damage can take place before mutations and aberrations are formed.[3–4] In cases where damage is gauged as too severe or irreparable, cells activate a programmed cell death response resulting in their elimination from the population. The accurate execution of the DNA damage response is not only important for preventing cancer, but also for treating cancer as many commonly used cancer chemotherapeutic agents function by generating DNA damage that preferentially induces death in fast growing cancer cells.[5]

[#]Corresponding author: 77 Massachusetts Avenue, 56-235, Cambridge, MA 02139, Phone: (617) 258-7813, Fax: (617) 253-8099, lsamson@mit.edu.

Methylating agents are an important class of chemotherapeutic DNA damaging agents currently in use in the cancer clinic.[6] The monofunctional S_N1 type methylating agent MNNG, like the chemotherapeutic agent temozolomide, produces a spectrum of DNA damage that includes over a dozen different methylated base lesions.[7] Although it makes up a small fraction of the overall DNA alkylation, the specific repair of O^6MeG by O^6MeG DNA methyltransferase (MGMT) prevents many of the detrimental effects of MNNG, pinpointing O^6MeG as the major genotoxic, cytotoxic, and carcinogenic lesion in cells treated with agents like MNNG and temozolomide.[8] MGMT directly repairs O^6MeG by transferring the methyl group from the O^6 position of guanine to an internal cysteine residue on the protein; such transfer causes a conformational change leading to MGMT's ubiquitin-mediated degradation.[9–11] If left unrepaired, O^6MeG preferentially mispairs with T during DNA replication ultimately giving rise to G:C to A:T transition mutations.[12–13] Importantly, O^6MeG-induced cytotoxicity is dependent on DNA mismatch repair (MMR), as cells deficient in this pathway are resistant to killing by S_N1 type methylating agents, especially in the absence of O^6MeG repair by MGMT.[14–15] With loss of MMR, cells become 'methylation tolerant', escaping cell death even though O^6MeG remains unrepaired; however, the cost of such tolerance is vastly increased sensitivity to the mutagenic and carcinogenic effects of methylating agents that produce O^6MeG lesions.[16]

The methylating agent MNNG is known to induce apoptotic cell death in an O^6MeG- and MMR-dependent manner.[17–21] Two models have been proposed for the mechanism of MMR-mediated sensitivity to this methylating agent, the direct signaling model and the futile repair model; it should be noted that the two models are not mutually exclusive. The first replication past an unrepaired O^6MeG lesion gives rise to an O^6MeG/T mismatch that can be recognized and bound by MutSα (MSH2/MSH6), followed by the recruitment of MutLα (MLH1/PMS2) to the mismatch.[22–24] In the direct signaling model, MMR proteins bound to the O^6MeG/T base pair are thought to directly activate a signaling kinase cascade that controls downstream events such as DNA repair, cell cycle arrest, and apoptosis. In support of this hypothesis, recruitment of the ATR protein kinase to the MutSα/MutLα-bound O^6MeG /T mismatch, accompanied by ATR kinase activation, was shown to occur *in vitro*.[23] In addition, it was demonstrated that a particular missense mutation in *Msh2* or *Msh6* uncouples the DNA repair function of MMR from its role in DNA damage-induced apoptosis, suggesting that excision of DNA opposite the O^6MeG lesion may not be required for the DNA damage response function of MMR.[25–26] Alternatively, it is thought that the futile rounds of excision and resynthesis of DNA at O^6MeG /T mismatches (on the newly synthesized T-containing strand) provide the trigger for activation of the DNA damage response. Following recognition of the mismatch by MutSα and MutLα, MMR initiates the excision and reinsertion of the nucleotides in the newly-synthesized daughter strand. Given that O^6MeG almost always directs the incorporation of T, iterative futile repair attempts by MMR would lead to secondary lesions in the DNA in the form of nicks and single strand gaps.[27] It is hypothesized that these nicks and gaps formed in the first S-phase after damage are encountered by replication forks in the next S-phase resulting in the blockage or collapse of DNA replication forks with ensuing DNA double strand break (DSB) formation. These DSBs in turn trigger a signaling response that activates the cell cycle checkpoint and the apoptotic signaling pathways. Multiple lines of evidence support this model. In agreement with the idea that a cell requires two rounds of replication to induce a DNA damage response, O^6MeG/MMR-dependent apoptosis and G2 cell cycle arrest have been shown to be activated only after the second S-phase following treatment with S_N1 type methylating agents.[28–30] Indeed, it was shown that MMR-dependent single-stranded gaps accumulate and persist in newly replicated DNA after MNNG treatment, providing *in vivo* evidence of iterative excision by MMR.[31] In addition, the importance of the excision step in inducing apoptosis was demonstrated using a mouse model deficient in the major MMR exonuclease, exonuclease 1 (Exo1); the absence of Exo1 conferred significant resistance to O^6MeG-

induced cell death, although the extent of resistance was cell type dependent.[32] Finally, the futile repair model is thought to lead to stalled replication forks at single strand breaks during the second S-phase. The stalled forks are ultimately rescued by recombination bypass or, in the event of fork collapse, give rise to DSBs that also require recombination in order to be resolved. Indeed, both sister chromatid exchanges (SCEs) and chromosome aberrations, two endpoints predicted by the futile repair model, are induced by the O^6MeG lesion in a MMR-dependent manner.[33] Importantly, the induction of SCEs and chromosome aberrations observed in these studies occurred almost exclusively in the second cell cycle post-treatment. In addition, the loss of homologous recombination grossly sensitizes cells to MNNG in an O^6MeG and MMR-dependent manner, suggesting that stalled replication forks and DSB lesions formed at O^6MeG/MMR-induced strand breaks are ordinarily resolved by homologous recombination.[34–36] Finally, it is important to note that while the futile repair model requires two S-phases to begin signaling the DNA damage response, direct signaling can, in principle, begin during the first S-phase after the induction of O^6MeG.

In this study, we made use of the TK6 human lymphoblastoid cell line and its isogenic derivatives TK6/MGMT$^+$ and TK6/MMR$^-$ to explore the O^6MeG/MMR-dependent signaling in more detail. It was previously shown that the O^6MeG DNA base lesion triggers a MMR-dependent apoptotic response in TK6 cells, and that this response is mediated at least in part by the mitochondrial signaling pathway.[37] Expression of the MGMT protein that specifically repairs the O^6MeG lesion in the TK6/MGMT$^+$ cells suppressed, in its entirety, the apoptotic response of TK6 cells upon treatment with the methylating agent MNNG. In addition, the MMR-deficient TK6-derivative cell line, TK6/MMR$^-$, was used to demonstrate that the O^6MeG-induced apoptotic response is entirely MMR dependent; the MMR-deficient phenotype of TK6/MMR$^-$ cells is caused by a mutation in MSH6 that disables the MutSα sliding clamp from translocating along the DNA, an important early event in the MMR process.[38–39] TK6/MMR$^-$ cells are resistant to MNNG despite the persistence of O^6MeG lesions in their DNA.[15, 40] Here we systematically investigated the cellular response of TK6 and its derivatives to the methylating agent N-methyl-N'-nitro-N-nitrosoguanidine (MNNG) to gain a better understanding of how cells coordinate cell cycle progression and cell death triggered by the critical DNA base lesion O^6MeG. Quantitative, dynamic measurements of the DNA signaling response were simultaneously obtained to further our understanding of the signaling events that trigger such cellular responses.

RESULTS

To explore the cell death decision mechanism triggered by O^6MeG, TK6 human lymphoblastoid cell line and its isogenic derivatives TK6/MGMT$^+$ and TK6/MMR$^-$ were treated with varying doses of the methylating agent MNNG. The treatment conditions examined include no (0 μg/ml; 0 μM), low dose (0.01 μg/ml; 0.068 μM), and high dose (0.1 μg/ml; 0.68 μM) MNNG. Concentrations were chosen to provide different levels of induction of O^6MeG- and MMR-dependent cell death. Current evidence suggests that cells require two rounds of replication to induce toxic lesions; therefore, phenotypic and signaling measurements were taken over a period of 48 hours post damage (TK6 cell doubling time 14–16 hours). Multiple molecular and cell behavioral endpoints were simultaneously examined to provide multi-variate insight into how DNA damage-induced cell behavior is regulated downstream of this chemotherapeutically-relevant DNA damage lesion.

MNNG inhibits cell growth in an O^6MeG/MMR-dependent manner

Treatment of TK6 cells with MNNG resulted in a dose-dependent inhibition of cell growth. The viable cell density of TK6 cells was monitored over time following exposure to MNNG (Figure 1A). We observed a significant decrease in the viable cell density (compared with untreated control cells) as early as 12 and 24 hours after treatment with a high and low

MNNG dose (0.1 and 0.01 μg/ml respectively) and this inhibition increased with time (Figure 1B). At 48 hours, TK6 control growth was 60 % and 19 % for low dose and high dose conditions, respectively (Figure 1B). The decreased cell growth was dependent on the persistence of O^6MeG lesions and on functional MMR as no growth inhibition was observed in MNNG-treated TK6/MGMT$^+$ or TK6/MMR$^-$ cells (Figures 1A and 1C). It is important to note that the viable cell density of untreated TK6 cells doubled within the first 16 hours of the time course and that this doubling was delayed following treatment with low dose (0.01 μg/ml) and high dose (0.1 μg/ml) MNNG (Figure 1A). This would suggest that the growth inhibition we observed at 12 hours is due to events occurring within the first cell cycle following treatment with MNNG (Figure 1B). Although delayed, the viable cell density of TK6 cells treated with low dose (0.01 μg/ml) MNNG doubled twice within the 48 hour time course experiment, once by 20 hours and again at 40 hours (Figure 1A), indicating cell division and progression into subsequent cell cycles. In contrast, when TK6 cells were treated with high dose (0.1 μg/ml) MNNG the viable cell density doubled only once. To gain more insight into the source of this DNA damage-induced growth inhibition we chose to look at the cellular responses of cell death and cell cycle progression in more detail.

MNNG induces O^6MeG/MMR-dependent apoptotic cell death in the second cell cycle

A study by Quiros *et al.* showed that MNNG-induced apoptosis in CHO-9 cells is a late event occurring only after cells pass through two replication cycles and enter their second G2/M-phase post MNNG treatment.[30] To examine the timing of the cell death response in TK6 cells, we monitored several distinct markers of apoptosis including caspase-3 and PARP cleavage, phosphatidylserine exposure, membrane permeability, and DNA fragmentation. An early event in apoptosis is the flipping of the phospholipid phosphatidylserine (PS) to the outer surface of the cell membrane. This translocation of PS was analyzed by flow cytometry using the phospholipid-binding protein annexin V as a probe to detect PS exposure in cells undergoing apoptosis. Staining with annexin V in combination with the vital dye 7AAD allowed us to distinguish between cells that were early apoptotic (annexin$^+$7AAD$^-$), mid apoptotic or necrotic (annexin$^+$7AAD$^+$), and late apoptotic or necrotic (annexin$^-$7AAD$^+$). Both mid to late apoptotic and necrotic cells lose their membrane integrity and stain positive for 7AAD. We observed a small but significant increase in the number of cells staining positive for annexin V and/or 7AAD (total cell death) as early as 24 hours after treatment with low dose (0.01 μg/ml) MNNG and 16 hours after treatment with high dose (0.1 μg/ml) MNNG (Figure 2A). Cell death increased steadily with time in a dose-dependent manner, with 11%, 30%, and 76% cell death at 48 hours for untreated, low dose MNNG, and high dose MNNG respectively (Figure 2A). Representative flow cytometry plots of untreated TK6 or TK6 treated with high dose MNNG are shown in Figure 2B. Although differentiation between necrosis and mid- to late-apoptosis could not be determined directly, detection of PS by annexin V preceded the loss of membrane integrity, providing evidence that the cell death observed in these studies is apoptotic rather than necrotic (illustrated in Figure 2C).

Caspases play a central role in the execution of apoptotic cell death, and we used flow cytometry to monitor the active form of the effector caspase, caspase-3, along with cleavage of its substrate, PARP. We observed a small yet significant increase in apoptosis in TK6 cells at 16 hours in response to both low (0.01 μg/ml) and high (0.1 μg/ml) doses of MNNG that increased with time in a dose-dependent manner (Figure 3A); in other words the increase in apoptosis with time was steeper at the high dose versus the low dose of MNNG. At 48 hours, cleaved (active) caspase-3 and/or cleaved (inactive) PARP levels (total apoptosis) was detected at 4%, 13%, and 68% for untreated, low dose MNNG, and high dose MNNG respectively (Figure 3A). Figure 3B shows the representative flow cytometry plots obtained for untreated TK6 and TK6 treated with high dose MNNG. Importantly, the

induction of apoptosis observed in TK6 cells was O^6MeG- and MMR-dependent, as TK6/MGMT$^+$ cells and TK6/MMR$^-$ cells did not display any significant increase in apoptosis following treatment with high dose (0.1 μg/ml) MNNG (Figure 3C). Another commonly used marker and hallmark of apoptotic cell death is the fragmentation of DNA. In agreement with the caspase-3 and PARP results, flow cytometry analysis of cells stained with propidium iodide (PI) showed a dose-dependent accumulation of subG1 DNA content beginning 16 hours after treatment with MNNG (Figure 4G); these results are discussed later in the context of other events in the cell cycle. In summary, using multiple methods of detection, we have demonstrated that O^6MeG and MMR-dependent apoptosis was triggered as cells entered the second cell cycle post MNNG treatment, supporting an indirect futile cycling model for mismatch repair-mediated signaling for cytotoxicity. With that being said, we observed a significant MNNG-induced reduction in viable cell density (compared to untreated cells) as early as 12 hours after high dose treatment (Figure 1B), several hours prior to the induction of apoptosis, leading us to hypothesize that additional behaviors besides cell death are influencing cell growth after MNNG treatment. Cells exposed to DNA damage undergo cell cycle arrest leading to a delay in cell cycle progression. To examine whether the growth inhibition we observed was brought about by a delay in cell cycle progression we monitored the dynamics of the cell cycle response in cells exposed to MNNG.

MNNG induces O^6MeG and MMR-dependent cell cycle perturbations in both the first and second cell cycle post treatment

To characterize the cell cycle response to DNA alkylation damage we monitored DNA content in combination with BrdU incorporation as a marker of active DNA replication following MNNG exposure. At various time points after the addition of MNNG, cells were pulse labeled with BrdU for one hour and subsequently analyzed both for the incorporation of BrdU into replicating DNA and for total DNA content. Coupling a measure of active replication with DNA content allowed us not only to visualize and quantitate cell cycle stage, but also to monitor cellular events during S-phase in more detail. Figure S1 depicts BrdU versus DNA content flow cytometry plots for a subset of time points analyzed in order to demonstrate the gating used to quantify the fraction of cells in each phase of the cell cycle. As shown, G1 and G2/M cells have 2N and 4N DNA content respectively. Using this method we could detect very early S-phase replicating cells even though they stain as G1 cells with PI, and we could detect very late S-phase replicating cells with apparent G2/M DNA content. Moreover, in mid S-phase it was possible to distinguish replicating and non-replicating cells by whether or not they had incorporated BrdU during the one hour pulse labeling time. As mentioned previously, subG1 DNA content was used as a measure of apoptotic cell death.

The visualization and detailed quantitation of cell cycle stage with time following treatment of TK6 cells with low and high doses of MNNG revealed interesting cell cycle dynamics (Figures 4A–H and S2). As early as eight hours after MNNG treatment TK6 cells showed a small but significant increase (p-value<0.01, two sample t-test comparing treated to untreated control) in the proportion of cells in mid S-phase (high dose) and G2/M-phase (low and high dose) of the cell cycle with a simultaneous dose-dependent decrease in the G1 population (Figures 4A–C). These data indicate a delay in cell cycle progression within the first cell cycle following treatment with MNNG and explains the observed delay in growth at early time points (Figure 1A). This initial checkpoint response appeared to dissolve by 16 hours as cells were observed to progress from S to G2/M and from G2/M to G1, indicated by a drop in mid S-phase (total) cells in parallel with an increase in the G2/M and G1 population at this time (Figures 4A–C; high dose). At 24 hours post treatment we observed a distinct accumulation of mid S-phase (total) cells under both low (0.01 μg/ml) and high (0.1

μg/ml) dose conditions compared with untreated cells (Figure 4B). Notably, at this time the number of viable cells under both treatment conditions had doubled suggesting that these cells are entering into the second S-phase post treatment (Figure 1A). Under low dose conditions this accumulation was transient and was followed by an increase in the G2/M and G1 fraction of cells at 32 and 40 hours respectively, indicating resumed progression through the cell cycle (Figures 4A and 4C). In support of cell cycle progression, the density of these cells reached a second doubling around 40 hours (Figure 1A). Following treatment with the high dose, cells showed an increased delay in S-phase compared to the low dose, with accumulation of total mid S-phase cells peaking at 32 hours (Figure 4B). In contrast to the low dose, the subsequent decrease of mid S-phase cells at late time points was not accompanied by an increase in the G2/M or G1 populations (Figures 4A and 4C); rather we observed a corresponding increase in cells with subG1 DNA content (Figure 4G). An increase in subG1 was also observed in cells treated with the low dose of MNNG, albeit to a lesser extent. It is important to note that the cell cycle perturbations that we observed in TK6 cells were O^6MeG- and MMR-dependent. Equivalent cell cycle analysis was carried out using TK6/MGMT$^+$ and TK6/MMR$^-$ cell lines following high dose treatment with MNNG (Figures S3–S6). Although a significant change (p-value<0.05, two sample t-test comparing treated to untreated control) was observed at eight hours in the G2/M- and early S-phase populations after high dose treatment in TK6/MGMT$^+$ cells, the perturbation was minimal and much smaller than that seen for TK6 cells (Figure S4). At all the subsequent time points, no significant differences were observed with high dose treatment compared to untreated cells in TK6/MGMT$^+$ cells (Figure S4). TK6/MMR$^-$ cells showed no significant differences between the untreated and treated conditions at any of the time points measured (Figure S6). From this analysis we have demonstrated that MNNG induces dynamic changes in all phases of the cell cycle and that all of these perturbations are O^6MeG- and MMR-dependent. Delays in cell cycle progression in response to DNA damage are brought about by the activation of cell cycle checkpoints that arrest cells in a particular cell cycle stage allowing time for DNA repair. Here we look more closely at several of these cell cycle checkpoints.

MNNG induces an early G2 arrest that delays but does not inhibit progression onto the next cell division

Previous studies have demonstrated a G2 arrest in the second, but not the first, cell cycle following MNNG treatment.[28, 30] To test whether the early cell cycle perturbations we observed in TK6 cells involved a *bona fide* G2 arrest, cells were stained with an antibody against the mitotic marker, phospho-histone H3, and mitotic cells were detected by flow cytometry (Figure 4I). As discussed previously, a small but significant increase (p-value<0.01, two sample t-test comparing treated to untreated control) in the percent of G2/M-phase cells was seen at eight hours following treatment with both low and high doses of MNNG (Figure 4C). At this time, we also detect a significant decrease (p-value<0.05, two sample t-test comparing treated to untreated control) in the proportion of mitotic cells staining positive for phospho-histone H3 (Figure 4I). This data suggests that shortly after MNNG treatment TK6 cells activate a G2 checkpoint preventing G2 cells from entering mitosis. However, this checkpoint appeared to be short-lived as the fraction of mitotic cells returned to untreated levels at 16 hours, accompanied by a corresponding movement of cells into G1 (compare high dose curves in Figures 4A and 4I). Cell division and the entrance of cells into G1 from G2 requires movement through mitosis; indeed the changes in phospho-histone H3 positive cells (mitotic cells) and G1-phase cells mirror each other throughout the time course experiment (compare Figures 4A and 4I). Although a transient G2 arrest cannot be eliminated in the second cell cycle, a strong delay in the progression of cells into G1 from G2/M at late time points was not evident following low dose treatment. Following the movement of cells into G2/M-phase from S-phase, we detected an increase in the fraction of phospho-histone H3 positive cells between 32 and 40 hours in parallel with as an increase in

the fraction of G1-phase cells at this time (compare low dose curves in Figures 4A and 4I). In addition, cell division and cell cycle progression after low dose treatment was supported by a second cell density doubling around 40 hours as discussed previously (Figure 1A). Under high dose conditions, cells did not appear to progress into G2/M from the second cell cycle S-phase but rather we observed an increase in the fraction of cells with subG1 DNA content at this time. In agreement with this, phospho-histone H3 levels remained low at late time points (Figure 4I). The observation that TK6 cells do not arrest in G2 of the second cell cycle in response to MNNG is in contrast to previous studies that show a dramatic accumulation of cells in this phase of the cell cycle.[28, 30] Here we observed that TK6 cells accumulate in mid S-phase of both the first and second cell cycle, and under high doses do not appear to escape the second S-phase indicating activation of an intra-S phase checkpoint that we chose to look into further.

MNNG induces an intra-S-phase arrest indicated by a reduction in S-phase DNA replication

In an effort to protect the genome, cells that encounter damage to their DNA during DNA replication can activate an intra-S-phase checkpoint. This checkpoint slows the progression of S-phase, allowing time for repair, both by suppressing the firing of late replication origins and by stabilizing stalled replication forks. As discussed previously, we observed an O^6MeG/MMR-dependent accumulation of cells in mid S-phase in both the first and second cell cycle following treatment with MNNG, suggesting activation of an intra-S-phase checkpoint (Figure 4B). To look more closely at the replication status of these cells, we divided the mid S-phase population into replicating and non-replicating populations defined by whether or not they incorporated BrdU during a one hour period prior to the time point indicated. Figures 4E and 4H break down the data in Figure 4B into replicating (4E) and non-replicating (4H) cells; note that the data look dramatically different in Figure 4E versus 4H, while 4B represents a composite. At late time points, we observed an increase in mid S-phase cells with impaired DNA replication following MNNG treatment (Figure 4H). To account for changes in the number of mid S-phase cells specifically, loss of replication potential is more clearly represented in Figure 5 that shows mid S $BrdU^-$ cells as a proportion of total mid S-phase cells as opposed to the proportion of total cells (as displayed in Figure 4). Beginning 16 and 24 hours after high dose and low dose treatment, respectively, we observed an increase in the fraction of TK6 cells in mid S-phase with grossly reduced BrdU incorporation, and the proportion of cells with such low replication activity increased with time in a dose-dependent manner (Figure 5). At 48 hours the majority (80%) of cells remaining in mid-S phase following treatment with high dose MNNG were not engaging in DNA replication (Figure 5). From this data it is clear that the DNA lesion O^6MeG provokes an intra-S phase checkpoint that, through either stalled replication forks or a reduction in the firing of replication origins (or both) results in a dose-dependent decrease in DNA replication, accompanied by the accumulation or trapping of cells in S-phase.

Apoptosis is specifically triggered out of the second cell cycle intra-S-phase arrest

Cell cycle analysis of TK6 cells treated with MNNG indicated an intra-S-phase arrest in both the first and second cell cycle post treatment (Figure 4). The second intra-S-phase arrest was marked by an increase in the overall S-phase population as well as a decrease in the replication status of those S-phase cells. Importantly, the second intra-S-phase arrest coincided with the induction of cell death via apoptosis. We hypothesized that the MNNG-induced intra-S-phase arrest in the second cell cycle, is accompanied by an inability to recover, and that this prompts cells to trigger apoptosis. To test the connection between triggering apoptosis and cell cycle stage we treated TK6 cells with MNNG and measured cleaved (active) caspase-3 in combination with DNA content. MNNG induced an increase in cleaved caspase-3 as cells entered the second cell cycle post treatment (>16 hours) and the majority of cleaved caspase-3 positive cells had S-phase or subG1 DNA content across all

time points (Figure 6A, Figure S7). At 40 hours, 92% of caspase-3 positive cells had either S phase or subG1 DNA content following treatment with high dose (0.1 μg/ml) MNNG (Figure 6A). The specificity for cell death out of S-phase is evident in Figure 6B, which depicts the cell population 32 hours after treatment with MNNG according to their cleaved caspase-3 and DNA content status. Under low dose conditions, a fraction of cells in S-phase showed an induction of apoptosis, illustrated by their positive cleaved caspase-3 status on the flow cytometry plot, while cells that had progressed through S into G2/M were negative for cleaved caspase-3 and therefore not undergoing caspase-dependent apoptosis (Figure 6B). Under high dose conditions, a similar but more pronounced S-phase-dependent activation of caspase-3 was observed (Figure 6B). It is important to note that a significant fraction of the subG1 population is negative for cleaved caspase-3 indicating a caspase-independent mode of apoptosis whose cell cycle origin cannot be accounted for using this assay (Figure S7, see 48 hour time point). Similar results were obtained for cleaved PARP (Figure S8). Overall, our results suggest that following cell cycle arrest, cells that have repairable or tolerable amounts of damage are able to avoid triggering apoptosis and are permitted to proceed through the cell cycle whereas if severe damage is uncovered during the S-phase of the second cell cycle post treatment with MNNG, cells are shunted directly into apoptosis without entering G2.

Quantitative temporal measurements of key DDR network proteins reveal MMR-dependent signaling dynamics triggered by the O^6MeG DNA lesion

We have demonstrated that MNNG induces O^6MeG/MMR-dependent cell cycle perturbations in TK6 cells not only in the second cell cycle following treatment, as expected, but also in the first cell cycle (Figure 4). In addition, while low levels of damage ultimately give rise to survival and progression into subsequent cell cycles, high levels of damage induce apoptotic cell death out of the second S-phase post treatment. To enhance our understanding of the O^6MeG/MMR-dependent cell cycle checkpoint and apoptotic cell death response induced by MNNG, we chose to monitor the activation or phosphorylation of a number of key signaling proteins thought to mediate such outcomes in response to DNA damage and replication stress. As described previously, TK6 cells were treated with various doses of MNNG and collected at specific time points post treatment for subsequent analysis. Quantitative western blotting was used to monitor dynamic changes in total- and phospho-protein levels while protein kinase activation was monitored directly using an IP kinase activity assay. The results presented below are based on the average of three independent time course experiments. Figure 7 provides an illustration of typical western blot results used for the quantitation shown in subsequent figures.

Following TK6 cell treatment with MNNG, we detected the phosphorylation of ATM(S1981), CHK1(S317), p53(S15), and p53(S20), as well as CHK2 kinase activation (Figure 8A–F). While evidence points to ATR playing a prominent role in the DNA damage response to MNNG, we do not have a good measure for its direct activation and therefore infer activity based on the phosphorylation of its downstream target CHK1 on the ATR-dependent residue serine-317.[41] In addition to the protein modifications mentioned, the stability of p53 appeared to be enhanced as we detected an MNNG-induced accumulation of total p53 with kinetics similar to its phosphorylation on serine-15 and serine-20 (Figure 9A). To address p53's primary role as a transcriptional regulator of genes we additionally assessed the levels of several well studied p53-regulated transcripts involved in apoptosis, cell cycle regulation, and DNA repair and found a similar pattern of induction between their expression and p53 protein levels with MNNG treatment (Figure 9B). Taken together these results suggest that p53 may play a transcriptional role in the regulation of cell behavior following MNNG treatment in TK6 cells though further studies are needed to determing p53's function in this context. In addition to the canonical DNA damage signaling proteins

just mentioned, the activation of several members of the MAPK pathway known to regulate various cellular processes in response to extracellular stimuli were monitored. While no or little activation of ERK or MK2 was observed, respectively, we did observe a dramatic induction of JNK in TK6 cells after treatment with MNNG (Figure 8G–I). To address whether the observed signaling events originated from MNNG-induced lesions other than O^6MeG, we repeated these experiments in TK6/MGMT$^+$ and TK6/MMR$^-$ cell lines. To our surprise, time course experiments in TK6/MGMT$^+$ and TK6/MMR$^-$ demonstrated that MNNG-induced activation of all of the signaling events tested, namely H2AX(S139), CHK1(S317), p53(S15 and S20), total p53, CHK2 kinase activation, and JNK kinase activation, were indeed triggered solely by the O^6MeG lesion in a MMR-dependent fashion across all time points monitored (Figures S9 and S10).

Though such signaling responses have been noted in previous studies in relation to the methylating agent MNNG, the quantitative and temporal approach taken here allows us to examine the timing of such events in further detail. For example, we observed a significant increase in the phosphorylation of ATM at serine-1981 above untreated levels beginning 16 hours after treatment with low dose (0.01 μg/ml) MNNG that, while minimal, remained upregulated up to 36 hours (Figure 8A). Interestingly, ATM (S1981) phosphorylation kinetics under high dose (0.1 μg/ml) conditions appeared biphasic with a detectable early response (0–16 hours) and more dramatic late response (16–36 hours) (Figure 8A). Of note, transition into the second phase occurred as cells began to enter their second cell cycle post treatment, at which time we observed the accumulation of cells in S phase, loss of DNA replication in S phase cells, and accumulation of apoptotic cells (Figure 4B, Figures 4H and 5, and Figure 4G respectively). We detected a pattern of phosphorylation similar to ATM for H2AX(S139), CHK1(S317), p53(S15) and p53(S20). That is, for each of these proteins, a modest yet significant increase in phosphorylation levels were observed at early (0–16 hours) time points followed by a more pronounced increase in phosphorylation levels at late (16–36 hours) time points (Figure 8B). In contrast, the induction of CHK2 and JNK kinase activation was significantly delayed. An increase in CHK2 activity above untreated levels was not detected until 20 and 28 hours after exposure to high dose (0.1 μg/ml) and low dose (0.01 μg/ml) MNNG, respectively, after which time CHK2 activation continued to rise (Figure 8D). Since we observed ATM phosphorylation immediately after cell exposure to MNNG, the lack of activation of CHK2, a downstream target of the ATM kinase, at early time points was unexpected. To confirm that the unexpected observation of delayed CHK2 activation was not due to differences in assay sensitivity (western blot versus kinase activity assay) we measured the phosphorylation of CHK2 at threonine-68 by western blot. Indeed, the phosphorylation of CHK2 at threonine-68 by western blot was detected in MNNG treated cells with the same kinetics to those seen with kinase activity measurements, confirming lack of CHK2 activation at early time points (Figure S11). Further, as with CHK2, our results demonstrated a delayed induction of JNK activation following MNNG treatment (Figure 8I); JNK activity increased beginning 12 hours and 20 hours after treatment with 0.1 μg/ml MNNG and 0.01 μg/ml MNNG, respectively, in the late phase after MNNG exposure.

DISCUSSION

In this study we take a systems-level approach towards achieving a more complete understanding of the cellular response to a chemotherapeutically-relevant class of DNA damaging agents, the S_N1 type methylating agents. Although S_N1 type methylating agents cause damage to numerous sites within DNA, as well as other macromolecules within the cell (e.g. RNA, lipids, proteins), it is well documented that the O^6MeG lesion, in the presence of a functional MMR pathway, is responsible for the toxic effects of these agents. However, the precise mechanism by which the MMR pathway triggers downstream events

like cell cycle arrest and apoptosis is less clear. Two models have been proposed that link the MMR pathway to S_N1 methylating agent sensitivity, a direct signaling model and an indirect futile repair model. Our results indicate that both may be working simultaneously to control cellular outcomes in response to the classical S_N1 type methylating agent MNNG.

In the direct signaling model, the recognition of an O^6MeG/T mismatch by MMR proteins is thought to provoke a signaling response through direct interaction between MMR proteins and key DNA damage signaling kinases. In this event, we would expect to observe a cellular response soon after MNNG treatment due to misincorporation of T opposite O^6MeG in the first S-phase. In support of this, we observed O^6MeG/MMR-dependent inhibition of cell growth and dynamic cell cycle changes in TK6 cells within the first cell cycle post MNNG treatment. Specifically, we detected an increase in the proportion of cells in S- and G2-phase of the cell cycle alongside a decrease in the proportion of cells in mitosis as early as eight hours following MNNG treatment, suggesting induction of a checkpoint response. It is important to keep in mind that this early checkpoint response is transient as cells are ultimately permitted to progress into subsequent cell cycles with unresolved DNA damage. Based on previous studies showing that a permanent G2 arrest is only sustained above a certain threshold of damage, it is possible that the MNNG damage signal is too low to induce a robust G2-M arrest in the first cell cycle post treatment.[42] Finally, we point out that the damage signal produced during the first round of replication is not sufficient to invoke cell death, as apoptosis is observed only after cells progress into their second round of replication.

Within the first cell cycle, we additionally detected a low persistent level of phosphorylation of a number of proteins involved in the DNA damage response, namely ATM, H2AX, CHK1, and p53, and this phosphorylation proved to be O^6MeG and MMR dependent. Previous studies have provided evidence that components of the MMR pathway, MutSα (MSH2/MSH6) and MutLα (MLH1/PMS2), physically interact with several of these signaling molecules in the presence and/or absence of DNA damage.[43–45] In a comprehensive study, MutSα and MutLα were found to directly interact with multiple components of the ATR-CHK1 signaling pathway, namely ATR, TOPBP1, and CHK1, and moreover the recruitment of these proteins to chromatin was enriched following treatment with MNNG.[46] In addition, it was demonstrated that the ATR protein kinase is recruited *in vitro* to O^6MeG/T mismatches in the presence of MMR proteins, resulting in ATR's activation and phosphorylation of its downstream target kinase CHK1.[23] As the ATR-CHK1 pathway is known for mediating cell cycle transitions in response to DNA lesions that give rise to replication protein A (RPA)-coated single-stranded DNA, including repair excision intermediates, we do not rule out the possibility that the CHK1 phosphorylation observed could originate from single-stranded DNA (ssDNA) gaps formed during MMR-mediated futile repair processing.[47] Along these lines, a study by Mojas *et al.* demonstrated that ssDNA gaps accumulate in cellular DNA within the first S-phase following treatment with MNNG in an MMR-dependent manner; but whether this is sufficient to invoke a signaling response is not clear.[31]

While substantial evidence supporting direct activation of the ATR-CHK1 pathway by MMR exists, a more unexpected result was the O^6MeG/MMR-dependent induction of phosphorylated ATM(S1981) within one hour after treatment with MNNG. ATM responds primarily to DSBs, an event that leads to its autophosphorylation at serine-1981 and activation.[48] However, the formation of DSBs is not expected to occur at such early time points following induction of the O^6MeG lesion. It is therefore important to point out that while ATM activation is often associated with DSB formation, it was shown that other forms of stress can activate ATM in a DSB-independent manner, in particular oxidative stress.[49] Additionally, ATM phosphorylation at serine-1981 was shown to be mediated by

ATR, and not by ATM autophosphorylation, following UV treatment or replication fork stalling.[50] Moreover, ATM has been shown to interact directly with the MMR protein MLH1, providing a mechanism for ATM localization to the site of damage indepenent of DSBs.[43] While the phosphorylation of ATM(S1981) is associated with ATM kinase activation and subsequent CHK2 phosphorylation, we did not detect CHK2 phosphorylation at threonine-68, nor did we detect CHK2 kinase activation, during this initial period of DDR signaling following MNNG treatment. From this study, we are unable to say whether the observed phosphorylation of ATM at serine-1981 is sufficent to trigger full kinase activation. Indeed, a number of post-translational modifications in addition to the phosphorylation at serine-1981 are required for the the complete activation of ATM.[51]

Distinct from the cell cycle effects observed at early time points, TK6 cells treated with MNNG undergo an O^6MeG/MMR-dependent intra-S-phase arrest in the second cell cycle that is marked by a dramatic accumulation of S-phase cells as well as a reduction in S-phase DNA replication. In addition, apoptotic cell death is triggered directly out of this second S-phase. That cells initiate such a response only after entering S-phase of the second cell cycle supports the futile repair model for MMR-induced O^6MeG cytotoxicity. According to this model, the futile repair of O^6MeG/T mismatches by MMR generates gapped DNA that interferes with DNA replication in the second S-phase, leading to fork collapse and double strand break formation, both of which are well known activators of the DDR network. Our results indicate a clear intra-S-phase arrest in the second cell cycle following both a low and high dose of MNNG. Further, we note that cells with low levels of damage, upon S-phase completion, continue through the second G2 without a prolonged cell cycle arrest. This result differs from previous studies that have demonstrated a dramatic accumulation of G2/M cells in the second cell cycle following treatment with both toxic and nontoxic doses of MNNG.[28, 30] We note that such differences could be attributed to differences in cell type. While our experiments were performed with TK6 human lymphoblastoid cells, reports indicating a G2 arrest after MNNG treatment utilized chinese hamster ovary CHO-9 and human embryonic kidney 293T cell lines, both of which have defective p53 functions.[28, 30] Most importantly, we were able to show for the first time a direct connection between cells in S-phase of the second cell cycle, where the toxic damage is presumed to form, and the initiation of cell death via apoptosis.

As described above, it is hypothesized that the ultimate trigger for cell death in response to MNNG is replication forks stalling, ultimately causing fork collapse and the formation of DSBs. In general, the ATM-CHK2 pathway is primarily activated in response to DSB lesions whereas the ATR-CHK1 pathway is activated by various lesions that give rise to ssDNA, like stalled replication forks and DSB repair intermediates. Based on the described model, all of these events (i.e. fork stalling, DSB formation, DSB repair intermediates) are presumed to take place in an MMR-dependent manner in the second S-phase following MNNG exposure. In agreement with this, our data show O^6MeG/MMR-dependent activation of both the ATM-CHK2 pathway and the ATR-CHK1 pathway that coincides perfectly with the accumulation of cells in the second S-phase. At this time, we detect the phosphorylation of ATM(S1981), H2AX(S139), CHK1(S317), and p53(S15 and S20), plus a dramatic increase in p53 levels, and CHK2 and JNK kinase activation. While many of the molecular players overlap between the first and second cell cycle response there are several key differences. For one, the damage signals triggered in the second S-phase are of a much greater magnitude than the damage signals triggered in the first cell cycle. Particularly with regard to the p53 tumor suppressor protein, the extent of DNA damage is an important factor in cellular outcome; low/transient stress induces a p53 transcriptional response that promotes ‘survival’ (i.e. genes involved in cell cycle arrest, DNA repair, metabolic homeostasis, etc.) while high/sustained levels of stress induces a p53 transcriptional response that promotes cell death or senescence.[52] Another difference between the early and late signaling response

is the activation of CHK2, which occurs only in the second cell cycle. While both CHK1 and CHK2 have roles in regulating cell cycle checkpoints in response to DNA damage, CHK2 plays a prominent role in the regulation of p53 and apoptosis in response to DSBs.[53] Therefore, we might speculate that with regard to MNNG, CHK2 mediates cell death while CHK1 serves a protective role by regulating cell cycle progression and DNA replication in the presence of persistent damage. In regards to this, Bartek and Lukas[53] coined CHK1 as a "workhorse" and CHK2 as an "amplifier" of the DDR. Interestingly, like CHK2, the stress-activated protein kinase JNK was activated by MNNG in an O^6MeG/MMR-dependent manner around the time that we also observed the accumulation of cells in S phase of the second cell cycle and accumulation of apoptotic cells. JNK has been implicated in the apoptotic response to a variety of stresses and therefore may be important for the induction of apoptosis following exposure to MNNG.[54]

Figure 10 depicts our model for O^6MeG/MMR-dependent cell cycle arrest and cell death according to the results discussed. Briefly, O^6MeG lesions are converted to O^6MeG/T mispairs in the first replication cycle. Subsequently, members of the MMR pathway, MutSα and MutLα, bind to the O^6MeG/T mismatch leading to direct activation of the DDR network that delays cell cycle progression through S- and G2- phase of the first cell cycle. In parallel, ssDNA gaps arise due to futile repair attempts by the MMR pathway. These gaps persist into the second cell cycle where they are encountered by replication forks in the second S-phase. Ultimately, this gives rise to stalled replication forks, fork collapse, and DSBs. Such events in turn trigger activation of the ATR-CHK1, ATM-CHK2, and JNK signaling pathways that together coordinate various cellular responses including an intra-S-phase arrest and, depending on the dose, either repair and survival, or apoptotic cell death.

EXPERIMENTAL

Cell Culture and Treatment Conditions

The TK6 B-lymphoblastoid cell line and its derivatives, TK6/MGMT$^+$ and MT1 (here referred to as TK6/MMR$^-$) have been described previously.[37] Cells were maintained in RPMI medium 1640 (Gibco #11875) supplemented with 10% equine serum, 2 mM L-glutamine, 100 units/ml penicillin, and 100 μg/ml streptomycin. Due to the large number of cells needed, time course experiments were performed in 1 L or 3 L spinner flasks. For drug treatment, logarithmically growing cells were split to a density of 3×10^5 cells/ml and MNNG, in 0.1 M sodium acetate (pH 5.0) was added directly to the culture medium. Cells were collected at the indicated time points and prepared as described for further analysis. Viable and total cell density were monitored using a Vi-cell XR cell viability analyzer (Beckman-Coulter) which determines cellular viability using a trypan blue exclusion test. Percent control growth was quantified as the percent viable cell density of treated cells compared to untreated control cells at the indicated time points post treatment.

Annexin V and 7AAD Staining

Cells were washed once with annexin binding buffer (ABB: 10 mM HEPES, 140 mM NaCl, 2.5 mM CaCl2, pH 7.4) and resuspended in 50 μl ABB containing PE-conjugated annexin V (1:25 dilution) and 7AAD (15 μg/ml). Cells were incubated for 15 minutes at room temperature. Following incubation, 250 μl of ABB was added to the cell suspension and analyzed immediately on a BD FACScan flow cytometer. 7-aminoactinomycin D (7AAD) (#A1310) and PE-conjugated annexin V (#A35111) were obtained from Molecular Probes.

Cleaved (Active) Caspase-3 and Cleaved (Inactive) PARP Detection

Cells were washed once in cold PBS and resuspended in 500 μl 4% paraformaldehyde in PBS (Electron Microscopy Sciences #15700). Cells were fixed for 15 minutes at room

temperature. After fixation, cells were washed with PBS and resuspended in 500 μl 100% methanol. Methanol suspensions were stored at −20°C. All antibody staining steps was performed in 96-well v-bottom plates. Fixed cells were resuspended in 200 μl PBS-B (PBS + 1% BSA) and blocked at room temperature for 30 minutes. Following incubation, cells were incubated in 100 μl of primary antibody diluted at 1:200 in PBS-TB (PBS-B + 0.1% Tween 20) for 1 hour at room temperature. Anti-cleaved (active) caspase-3 antibody (#559565) and anti-cleaved (inactive) PARP antibody (#552597) were purchased from BD Biosciences. Following primary antibody incubation, cells were washed twice with PBS-T (PBS + 0.1% Tween 20). Cells were then resuspended in 100 μl PBS-TB containing secondary antibody diluted at 1:600 and incubated for 1 hour at room temperature. The secondary antibodies used, PE-conjugated goat anti-rabbit IgG (#P2771) and Alexa Fluor 647-conjugated goat anti-mouse IgG (#A21235), were purchased from Molecular Probes. Finally, cells were washed twice with PBS-T, resuspended in 100 μl PBS-TB, and analyzed on a BD FACSCalibur flow cytometer.

Simultaneous Detection of DNA Content and Apoptotic Markers

For the simultaneous detection of DNA content and apoptosis, cells were fixed and stained for cleaved (active) casapase-3 and cleaved (inactive) PARP as described above. Following secondary antibody incubation, cells were washed once with PBS-T (PBS + 0.1% Tween 20) and resuspended in 200 μl Hoechst 33258 (10 mg/ml stock solution, Invitrogen) at 1:10,000 dilution in PBS. Cells were incubated in Hoechst 33258 for 10 minutes at room temperature in the dark. Finally, cells were washed with PBS-T and resuspended in 120 μl PBS-TB (PBS-T + 1% BSA) for analysis on a FACS LSR II flow cytometer.

Detection of Mitotic Cells – Phospho Histone H3 and DNA Content

Cells were washed once in cold PBS and resuspended in 500 μl 4% paraformaldehyde in PBS (Electron Microscopy Sciences #15700). Cells were fixed for 15 minutes at room temperature. After fixation, cells were washed with PBS and resuspended in 500 μl 100% methanol. Methanol suspensions were stored at −20°C. Fixed cells were washed once with PBS followed by permeabilization with Triton X-100. For permeabilization, cells were suspended in 400 μl of PBS + 0.25% Triton X-100 for 15 minutes at room temperature. Afterwards, cells were washed with PBS-B (PBS + 1% BSA) and resuspended in 100 μl PBS-B containing primary antibody against phosphorylated Histone H3 (0.75 μg). Anti-phospho-Histone H3 (Ser 10) antibody was purchased from Upstate (#06-570). Cells were incubated with primary antibody for three hours at room temperature. Following antibody incubation, cells were washed twice with PBS-B and incubated with Alexa Flour 647-conjugated goat anti-rabbit IgG antibody (Molecular Probes #A21244) diluted in 100 μl PBS-B (1:30) for 30 minutes at room temperature. Finally, cells were washed twice with PBS and resuspended in 1 ml PBS containing 50 μg propidium iodide (Molecular Probes # P21493) and 500 μg RNase A (Sigma #R6513). Cells were analyzed on a BD FACSCalibur flow cytometer for phospho-Histone H3 detection and DNA content.

Detection of DNA Synthesis – BrdU Incorporation and DNA content

One hour before cell collection, BrdU was added to the culture medium at a concentration of 10 μM. At the corresponding time point, cells were collected, washed with cold PBS, and resuspended in 500 μl cold PBS. Cells were fixed by adding 5 ml ethanol (-20°C) while vortexing to prevent clumping and stored at 4°C overnight. In order to provide access to the incorporated BrdU, partial DNA denaturation was needed prior to staining with anti-BrdU antibody. Fixed cells were washed with PBS-B (PBS + 1% BSA) and incubated in 1 ml 2 M HCl + 0.5% Triton X-100 for 30 minutes at room temperature, followed by incubation in 1 ml 0.1 M $Na_2B_4O_7$ for 2 minutes at room temperature. Next, cells were washed in PBS-TB (PBS-B + 0.5% Tween 20) and resuspended with anti-BrdU antibody (BD Biosciences

#555627) diluted in 60 μl PBS-TB (5 μg antibody per approx 5×10^6 cells) and incubated at room temperature for 2 hours. Cells were washed twice with PBS-T (PBS + 0.5% Tween 20) and resuspended in 55 μl PBS-T containing 5 μl Alexa Fluor 647-conjugated goat anti-mouse IgG antibody (1:11 dilution, 10 μg of antibody per approx 5×10^6 cells). Cells were incubated with secondary antibody for 1 hour at room temperature (Molecular Probes #A21235). Cells were then washed twice with PBS-T and resuspended in 1 ml PBS containing 50 μg propidium iodide (Molecular Probes # P21493) and 500 μg RNase A (Sigma #R6513). Cells were analyzed on a BD FACSCalibur flow cytometer for BrdU detection and DNA content.

Preparation of Cell Extracts

Cells were washed with cold PBS and lysed in 1% Triton X-100, 50 mM Tris-HCl (pH 7.5), 150 mM sodium chloride, 50 mM β-glycerophosphate (pH 7.3), 10 mM sodium pyrophosphate, 30 mM sodium fluoride, 1 mM benzamidine, 2 mM EGTA, 100 μM sodium orthovanadate ($NaVO_4$), 1 mM dithiothreitol (DTT), 1 mM phenylmethylsulfonyl fluoride (PMSF), 10 μg/ml aprotinin, 10 μg/ml leupeptin, 1 μg/ml pepstatin, 1 μg/ml microcystin-LR. Lysates were incubated on ice for 30 minutes, and clarified by centrifugation at max speed (16110×g) for 10 minutes at 4°C. Protein concentrations of clarified extracts were determined using the BCA protein assay (Pierce). Lysates prepared for western blotting were sonicated (Branson Model 450 Digital Sonifier: Amplitude 20%, Pulse Time 2 seconds, Repeat 3×) prior to centrifugation.

Kinase Activity Assay

A microtiter-based assay was used in these studies to monitor protein kinase activity following DNA damage. The assay was adapted from Janes *et al.*[55] who monitored various kinase activities to identify critical nodes within the signaling network regulating cytokine-induced apoptosis.[56] The assay is divided into three parts: immunoseparation of the kinase in microtiter wells; *in vitro* kinase reaction; and measurement of ^{32}P incorporation into the substrate. A detailed description of the experimental procedure was published previously[55] and will be described here briefly along with any adjustments made to the original protocol. Protein A or G coated microtiter wells were incubated overnight at 4°C with 10 μg/ml antibody against the kinase of interest. The following antibodies were used to perform the immunoprecipitation step: Anti-MAP Kinase 1/2 (Erk1/2), CT (Upstate #06-182), Anti-JNK1 (C-17) (Santa Cruz Biotechnology #sc-474), Anti-MAPKAPK-2 (Stressgen #KAP-MA015), Anti-Chk2 (Bethyl Laboratories #BL1432). The next day, wells were washed and incubated with cell lysate (150 μg for CHK2, 37.5 μg for ERK, 150 μg for JNK, and 150 μg for MK2) for three hours at 4°C. After being washed, the wells were filled with kinase buffer containing cold ATP and [^{32}P]ATP along with the kinase-specific substrate. The substrate along with the concentration of cold ATP and [^{32}P]ATP used in each kinase reaction can be found in Table S1. The substrates include myelin basic protein (purchased from Sigma #M1891), MK2tide (described in [57]), and GST-ATF2 (1–109) (described in [58]). Following incubation at 37°C for one hour, the reaction was quenched with 20 mM EDTA or 75 mM phosphoric acid depending on the kinase being tested (see Table S1). The contents were then applied to a 96-well phosphocellulose filter to capture the phosphorylated substrate. After repeated washings, the filter was punched into scintillation vials and the [^{32}P]substrate was measured by liquid scintillation counting. The linearity and range of the assay, as well as its sensitivity to external stimuli, was tested in our model system for each of the protein kinases monitored in this study. All measurements were normalized to a positive control in order to control for day to day assay variability; results are reported as fold activation above untreated background levels (activity at 0 hours).

Quantitative Western Blot

Regulatory phosphorylation events and total protein levels of several key DNA damage signaling proteins were monitored by quantitative western blotting. Whole cell lysates were prepared at a concentration of 2.5 mg/ml in sample buffer, containing 1X LDS (Lithium Dodecyl Sulfate) Sample Buffer (NuPage, Invitrogen) and 2.5% β-mercaptoethanol, and heated at 80°C for 10 minutes. Protein samples were separated by SDS-PAGE using the NuPage Electrophoresis System (Invitrogen), and transferred to a PVDF or nitrocellulose membrane in transfer buffer (49.1 mM TrisBase, 38.6 mM Glycine, 0.04% SDS, 20% Methanol) for one hour at 100V using a Criterion Blotter (BioRad). After the transfer, membranes were blocked at room temperature for one hour with Odyssey Blocking Buffer (OBB, Licor Biosciences) and then probed with primary antibodies. Primary antibodies were diluted in a 1:1 mixture of OBB:PBS-T (PBS + 0.1% Tween 20) and incubated with the membrane overnight at 4°C. Following repeated washes with PBS-T, IRDye secondary antibodies (Licor Biosciences) were diluted in a 1:1 mixture of OBB:PBS-T (1:5000-1:10000 dilution) and incubated with the membrane for one hour at room temperature covered from light. The membrane was washed again in PBS-T and stored in PBS at 4°C in the dark until detection using the Odyssey Infrared Imaging System (Licor Biosciences). Using the Odyssey's two-color detection system we were able to detect both phopho- and total- antigen targets simultaneously by probing with secondary antibodies that could be visualized in different fluorescence channels. Following protein detection, membranes were stained with actin antibody which was used as a loading control. The specific immunoblot conditions for each of the proteins detected are described in Table S2. Antibodies were tested for linearity and sensitivity using a positive control. Positive controls were run on every gel and signal intensities were normalized to the intensity of the reference sample to correct for differences in transfer and probing efficiencies. Each time course is reported as fold change above untreated background levels (signal at 0 hours).

RNA Isolation and Microarray Hybridization

TK6 cells were treated with 0 μg/ml, 0.01 μg/ml, or 0.1 μg/ml MNNG as described and collected at various time points following exposure to the drug. Total RNA was extracted from cells with TRIZOL reagent (Invitrogen) and purified using Qiagen's RNeasy Mini Kit. Evaluation of sample quality was performed on the Agilent 2100 BioAnalyzer (BioMicro Center, MIT). Sample labeling, array hybridization, and data extraction were performed by the BioMicro Center (MIT). RNA was hybridized to HGU133 Plus 2.0 full human genome arrays (Affymetrix). Data normalization was performed in GenePattern.[59] Affymetrix CEL files were uploaded to GenePattern (ExpressionFileCreator module) which was then used to carry out quantile normalization using the Robust Multichip Average (RMA) algorithm.

Supplementary Material

Refer to Web version on PubMed Central for supplementary material.

Acknowledgments

The authors would like to thank Gerard Ostheimer for help in the initial phases of this project. The authors have been supported by US National Institutes of Health grants CA112967, CA055042, CA 014051 and ES002109. L.D.S. is an American Cancer Society Research Professor.

REFERENCES

1. Ciccia A, Elledge SJ. The DNA damage response: making it safe to play with knives. Mol Cell. 2010; 40:179–204. [PubMed: 20965415]

2. Hoeijmakers JH. Genome maintenance mechanisms for preventing cancer. Nature. 2001; 411:366–374. [PubMed: 11357144]
3. Zhou BB, Elledge SJ. The DNA damage response: putting checkpoints in perspective. Nature. 2000; 408:433–439. [PubMed: 11100718]
4. Harper JW, Elledge SJ. The DNA damage response: ten years after. Mol Cell. 2007; 28:739–745. [PubMed: 18082599]
5. Jackson SP, Bartek J. The DNA-damage response in human biology and disease. Nature. 2009; 461:1071–1078. [PubMed: 19847258]
6. Drablos F, Feyzi E, Aas PA, Vaagbo CB, Kavli B, Bratlie MS, Pena-Diaz J, Otterlei M, Slupphaug G, Krokan HE. Alkylation damage in DNA and RNA--repair mechanisms and medical significance. DNA Repair (Amst). 2004; 3:1389–1407. [PubMed: 15380096]
7. Beranek DT. Distribution of methyl and ethyl adducts following alkylation with monofunctional alkylating agents. Mutat Res. 1990; 231:11–30. [PubMed: 2195323]
8. Kaina B, Christmann M, Naumann S, Roos WP. MGMT: key node in the battle against genotoxicity, carcinogenicity and apoptosis induced by alkylating agents. DNA Repair (Amst). 2007; 6:1079–1099. [PubMed: 17485253]
9. Pegg AE. Repair of O(6)-alkylguanine by alkyltransferases. Mutat Res. 2000; 462:83–100. [PubMed: 10767620]
10. Margison GP, Santibanez-Koref MF. O6-alkylguanine-DNA alkyltransferase: role in carcinogenesis and chemotherapy. Bioessays. 2002; 24:255–266. [PubMed: 11891762]
11. Gerson SL. MGMT: its role in cancer aetiology and cancer therapeutics. Nat Rev Cancer. 2004; 4:296–307. [PubMed: 15057289]
12. Altshuler KB, Hodes CS, Essigmann JM. Intrachromosomal probes for mutagenesis by alkylated DNA bases replicated in mammalian cells: a comparison of the mutagenicities of O4-methylthymine and O6-methylguanine in cells with different DNA repair backgrounds. Chem Res Toxicol. 1996; 9:980–987. [PubMed: 8870985]
13. Delaney JC, Essigmann JM. Context-dependent mutagenesis by DNA lesions. Chem Biol. 1999; 6:743–753. [PubMed: 10508678]
14. Branch P, Aquilina G, Bignami M, Karran P. Defective mismatch binding and a mutator phenotype in cells tolerant to DNA damage. Nature. 1993; 362:652–654. [PubMed: 8464518]
15. Goldmacher VS, Cuzick RA Jr, Thilly WG. Isolation and partial characterization of human cell mutants differing in sensitivity to killing and mutation by methylnitrosourea and N-methyl-N'-nitro-N-nitrosoguanidine. J Biol Chem. 1986; 261:12462–12471. [PubMed: 3745200]
16. Karran P. Mechanisms of tolerance to DNA damaging therapeutic drugs. Carcinogenesis. 2001; 22:1931–1937. [PubMed: 11751422]
17. Tominaga Y, Tsuzuki T, Shiraishi A, Kawate H, Sekiguchi M. Alkylation-induced apoptosis of embryonic stem cells in which the gene for DNA-repair, methyltransferase, had been disrupted by gene targeting. Carcinogenesis. 1997; 18:889–896. [PubMed: 9163672]
18. Kaina B, Ziouta A, Ochs K, Coquerelle T. Chromosomal instability, reproductive cell death and apoptosis induced by O6-methylguanine in Mex-, Mex+ and methylationtolerant mismatch repair compromised cells: facts and models. Mutat Res. 1997; 381:227–241. [PubMed: 9434879]
19. Meikrantz W, Bergom MA, Memisoglu A, Samson L. O6-alkylguanine DNA lesions trigger apoptosis. Carcinogenesis. 1998; 19:369–372. [PubMed: 9498291]
20. Hickman MJ, Samson LD. Role of DNA mismatch repair and p53 in signaling induction of apoptosis by alkylating agents. Proc Natl Acad Sci U S A. 1999; 96:10764–10769. [PubMed: 10485900]
21. Takagi Y, Takahashi M, Sanada M, Ito R, Yamaizumi M, Sekiguchi M. Roles of MGMT and MLH1 proteins in alkylation-induced apoptosis and mutagenesis. DNA Repair (Amst). 2003; 2:1135–1146. [PubMed: 13679151]
22. Duckett DR, Drummond JT, Murchie AI, Reardon JT, Sancar A, Lilley DM, Modrich P. Human MutSalpha recognizes damaged DNA base pairs containing O6- methylguanine, O4-methylthymine, or the cisplatin-d(GpG) adduct. Proc Natl Acad Sci U S A. 1996; 93:6443–6447. [PubMed: 8692834]

23. Yoshioka K, Yoshioka Y, Hsieh P. ATR kinase activation mediated by MutSalpha and MutLalpha in response to cytotoxic O6-methylguanine adducts. Mol Cell. 2006; 22:501–510. [PubMed: 16713580]
24. Warren JJ, Pohlhaus TJ, Changela A, Iyer RR, Modrich PL, Beese LS. Structure of the human MutSalpha DNA lesion recognition complex. Mol Cell. 2007; 26:579–592. [PubMed: 17531815]
25. Lin DP, Wang Y, Scherer SJ, Clark AB, Yang K, Avdievich E, Jin B, Werling U, Parris T, Kurihara N, Umar A, Kucherlapati R, Lipkin M, Kunkel TA, Edelmann W. An Msh2 point mutation uncouples DNA mismatch repair and apoptosis. Cancer Res. 2004; 64:517–522. [PubMed: 14744764]
26. Yang G, Scherer SJ, Shell SS, Yang K, Kim M, Lipkin M, Kucherlapati R, Kolodner RD, Edelmann W. Dominant effects of an Msh6 missense mutation on DNA repair and cancer susceptibility. Cancer Cell. 2004; 6:139–150. [PubMed: 15324697]
27. York SJ, Modrich P. Mismatch repair-dependent iterative excision at irreparable O6-methylguanine lesions in human nuclear extracts. J Biol Chem. 2006; 281:22674–22683. [PubMed: 16772289]
28. Stojic L, Mojas N, Cejka P, Di Pietro M, Ferrari S, Marra G, Jiricny J. Mismatch repair-dependent G2 checkpoint induced by low doses of SN1 type methylating agents requires the ATR kinase. Genes Dev. 2004; 18:1331–1344. [PubMed: 15175264]
29. Caporali S, Falcinelli S, Starace G, Russo MT, Bonmassar E, Jiricny J, D'Atri S. DNA damage induced by temozolomide signals to both ATM and ATR: role of the mismatch repair system. Mol Pharmacol. 2004; 66:478–491. [PubMed: 15322239]
30. Quiros S, Roos WP, Kaina B. Processing of O6-methylguanine into DNA doublestrand breaks requires two rounds of replication whereas apoptosis is also induced in subsequent cell cycles. Cell Cycle. 2010; 9:168–178. [PubMed: 20016283]
31. Mojas N, Lopes M, Jiricny J. Mismatch repair-dependent processing of methylation damage gives rise to persistent single-stranded gaps in newly replicated DNA. Genes Dev. 2007; 21:3342–3355. [PubMed: 18079180]
32. Klapacz J, Meira LB, Luchetti DG, Calvo JA, Bronson RT, Edelmann W, Samson LD. O6-methylguanine-induced cell death involves exonuclease 1 as well as DNA mismatch recognition in vivo. Proc Natl Acad Sci U S A. 2009; 106:576–581. [PubMed: 19124772]
33. Kaina B. Mechanisms and consequences of methylating agent-induced SCEs and chromosomal aberrations: a long road traveled and still a far way to go. Cytogenet Genome Res. 2004; 104:77–86. [PubMed: 15162018]
34. Nowosielska A, Smith SA, Engelward BP, Marinus MG. Homologous recombination prevents methylation-induced toxicity in Escherichia coli. Nucleic Acids Res. 2006; 34:2258–2268. [PubMed: 16670432]
35. Cejka P, Jiricny J. Interplay of DNA repair pathways controls methylation damage toxicity in Saccharomyces cerevisiae. Genetics. 2008; 179:1835–1844. [PubMed: 18579505]
36. Roos WP, Nikolova T, Quiros S, Naumann SC, Kiedron O, Zdzienicka MZ, Kaina B. Brca2/Xrcc2 dependent HR, but not NHEJ, is required for protection against O(6)-methylguanine triggered apoptosis, DSBs and chromosomal aberrations by a process leading to SCEs. DNA Repair (Amst). 2009; 8:72–86. [PubMed: 18840549]
37. Hickman MJ, Samson LD. Apoptotic signaling in response to a single type of DNA lesion, O(6)-methylguanine. Mol Cell. 2004; 14:105–116. [PubMed: 15068807]
38. Iaccarino I, Marra G, Dufner P, Jiricny J. Mutation in the magnesium binding site of hMSH6 disables the hMutSalpha sliding clamp from translocating along DNA. J Biol Chem. 2000; 275:2080–2086. [PubMed: 10636912]
39. Szadkowski M, Iaccarino I, Heinimann K, Marra G, Jiricny J. Characterization of the mismatch repair defect in the human lymphoblastoid MT1 cells. Cancer Res. 2005; 65:4525–4529. [PubMed: 15930269]
40. Kat A, Thilly WG, Fang WH, Longley MJ, Li GM, Modrich P. An alkylationtolerant, mutator human cell line is deficient in strand-specific mismatch repair. Proc Natl Acad Sci U S A. 1993; 90:6424–6428. [PubMed: 8341649]

41. Nam EA, Cortez D. ATR signalling: more than meeting at the fork. Biochem J. 2011; 436:527–536. [PubMed: 21615334]
42. Krempler A, Deckbar D, Jeggo PA, Lobrich M. An imperfect G2M checkpoint contributes to chromosome instability following irradiation of S and G2 phase cells. Cell Cycle. 2007; 6:1682–1686. [PubMed: 17637566]
43. Brown KD, Rathi A, Kamath R, Beardsley DI, Zhan Q, Mannino JL, Baskaran R. The mismatch repair system is required for S-phase checkpoint activation. Nat Genet. 2003; 33:80–84. [PubMed: 12447371]
44. Wang Y, Qin J. MSH2 and ATR form a signaling module and regulate two branches of the damage response to DNA methylation. Proc Natl Acad Sci U S A. 2003; 100:15387–15392. [PubMed: 14657349]
45. Adamson AW, Beardsley DI, Kim WJ, Gao Y, Baskaran R, Brown KD. Methylator-induced, mismatch repair-dependent G2 arrest is activated through Chk1 and Chk2. Mol Biol Cell. 2005; 16:1513–1526. [PubMed: 15647386]
46. Liu Y, Fang Y, Shao H, Lindsey-Boltz L, Sancar A, Modrich P. Interactions of human mismatch repair proteins MutSalpha and MutLalpha with proteins of the ATRChk1 pathway. J Biol Chem. 2010; 285:5974–5982. [PubMed: 20029092]
47. Cimprich KA, Cortez D. ATR: an essential regulator of genome integrity. Nat Rev Mol Cell Biol. 2008; 9:616–627. [PubMed: 18594563]
48. Bakkenist CJ, Kastan MB. DNA damage activates ATM through intermolecular autophosphorylation and dimer dissociation. Nature. 2003; 421:499–506. [PubMed: 12556884]
49. Guo Z, Kozlov S, Lavin MF, Person MD, Paull TT. ATM activation by oxidative stress. Science. 2010; 330:517–521. [PubMed: 20966255]
50. Stiff T, Walker SA, Cerosaletti K, Goodarzi AA, Petermann E, Concannon P, O'Driscoll M, Jeggo PA. ATR-dependent phosphorylation and activation of ATM in response to UV treatment or replication fork stalling. EMBO J. 2006; 25:5775–57782. [PubMed: 17124492]
51. Derheimer FA, Kastan MB. Multiple roles of ATM in monitoring and maintaining DNA integrity. FEBS Lett. 2010; 584:3675–3681. [PubMed: 20580718]
52. Vousden KH, Prives C. Blinded by the Light: The Growing Complexity of p53. Cell. 2009; 137:413–431. [PubMed: 19410540]
53. Bartek J, Lukas J. Chk1 and Chk2 kinases in checkpoint control and cancer. Cancer Cell. 2003; 3:421–429. [PubMed: 12781359]
54. Dhanasekaran DN, Reddy EP. JNK signaling in apoptosis. Oncogene. 2008; 27:6245–6251. [PubMed: 18931691]
55. Janes KA, Albeck JG, Peng LX, Sorger PK, Lauffenburger DA, Yaffe MB. A high-throughput quantitative multiplex kinase assay for monitoring information flow in signaling networks: application to sepsis-apoptosis. Mol Cell Proteomics. 2003; 2:463–473. [PubMed: 12832460]
56. Janes KA, Albeck JG, Gaudet S, Sorger PK, Lauffenburger DA, Yaffe MB. A systems model of signaling identifies a molecular basis set for cytokine-induced apoptosis. Science. 2005; 310:1646–1653. [PubMed: 16339439]
57. Manke IA, Nguyen A, Lim D, Stewart MQ, Elia AE, Yaffe MB. MAPKAP kinase-2 is a cell cycle checkpoint kinase that regulates the G2/M transition and S phase progression in response to UV irradiation. Mol Cell. 2005; 17:37–48. [PubMed: 15629715]
58. Gupta S, Campbell D, Derijard B, Davis RJ. Transcription factor ATF2 regulation by the JNK signal transduction pathway. Science. 1995; 267:389–393. [PubMed: 7824938]
59. Reich M, Liefeld T, Gould J, Lerner J, Tamayo P, Mesirov JP. GenePattern 2.0. Nat Genet. 2006; 38:500–501. [PubMed: 16642009]

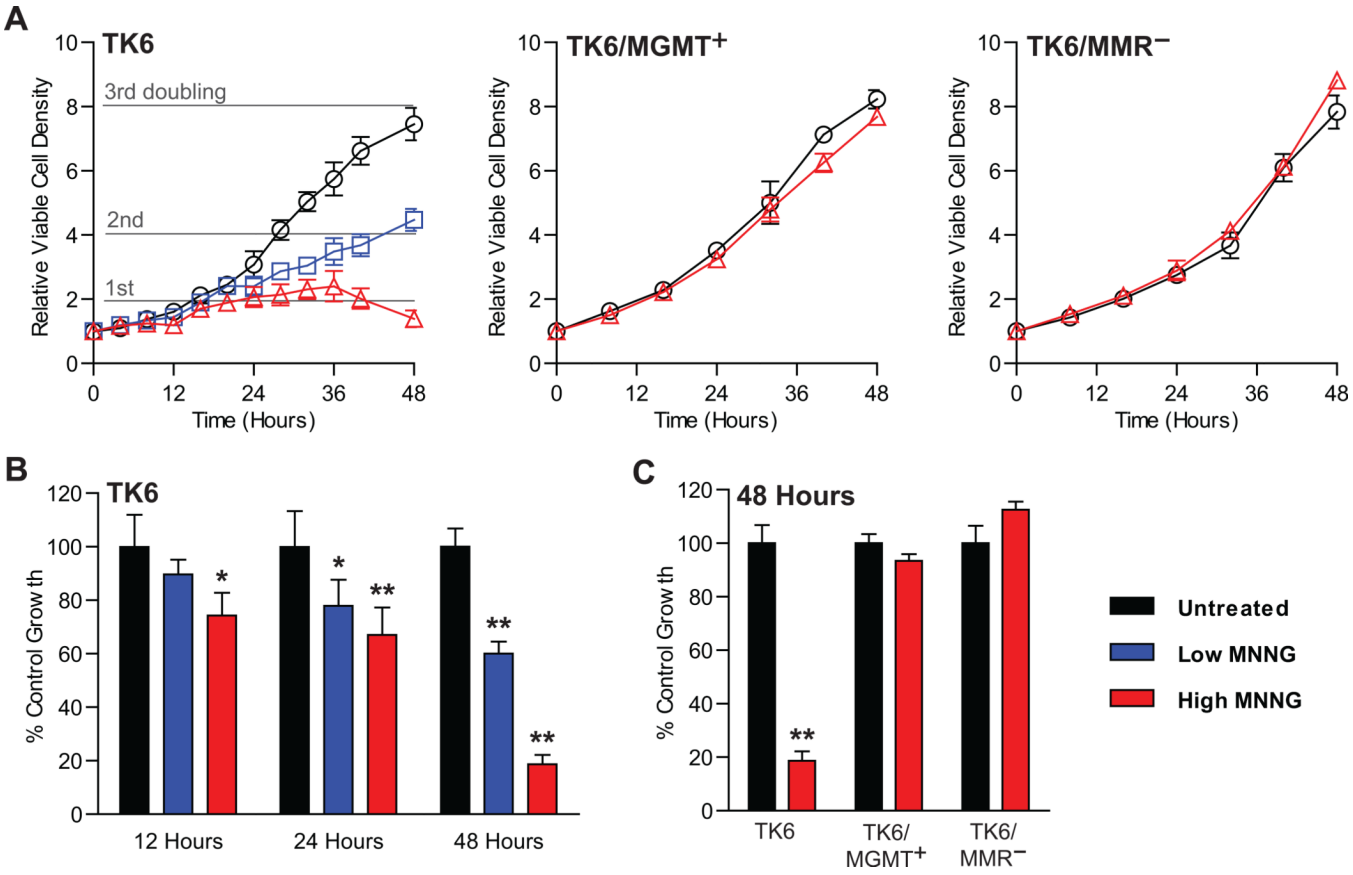

Figure 1. MNNG treatment leads to a dose-dependent inhibition of cell growth

(A) Viable cell density was monitored over time after treatment with 0 μg/ml (⊖), 0.01 μg/ml (⊟), or 0.1 μg/ml (△) MNNG for TK6, TK6/MGMT$^+$, and TK6/MMR$^-$ cells. Results are normalized to the 0 hour time point and plotted as 'Relative Viable Cell Density'. (B) Percent control growth of TK6 cells at 12, 24, and 48 hours after treatment with 0 μg/ml (black bars), 0.01 μg/ml (blue bars), and 0.1 μg/ml (red bars) MNNG. Results represent the percent viable cell density of treated cells compared to untreated control cells. *p<0.05, **p<0.01 (two sample t-test), when comparing treated cells to untreated control cells at the indicated time point. (C) Percent control growth of TK6, TK6/MGMT$^+$, and TK6/MMR$^-$ cells at 48 hours following treatment with 0 μg/ml (black bars) or 0.1 μg/ml (red bars) MNNG. Results represent the percent viable cell density of treated cells compared to untreated control cells. *p<0.05, **p<0.01 (two sample t-test), when comparing treated cells to untreated control cells at the indicated time point. For all panels, the means and standard deviations for independent experimental replicates are shown (error bars appear absent when they are smaller than the symbol).

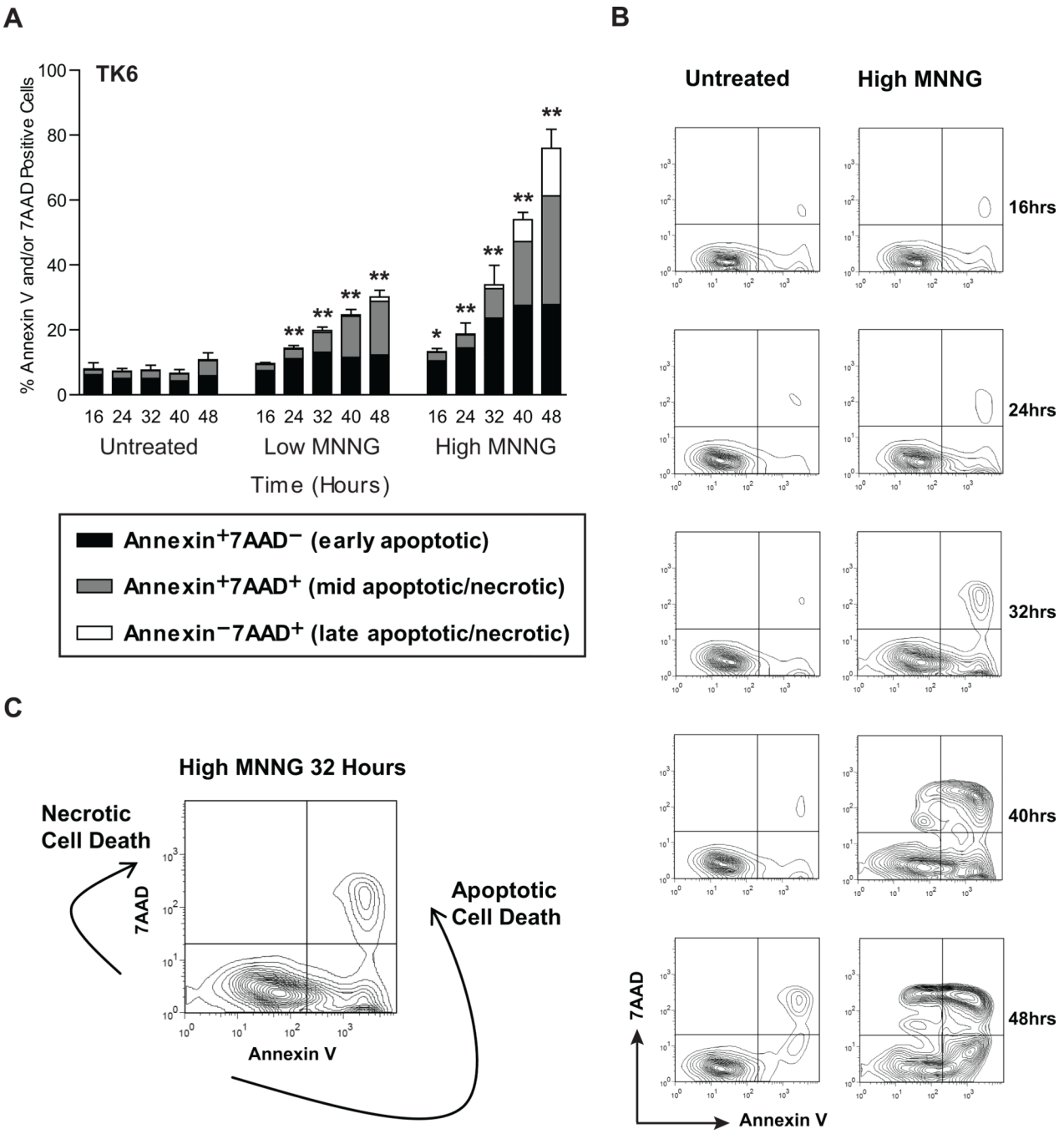

Figure 2. MNNG induces apoptotic cell death in TK6 cells

TK6 cell death was analyzed at specific time points following 0 μg/ml, 0.01 μg/ml (low dose), or 0.1 μg/ml (high dose) MNNG. Flow cytometry was used to simultaneous detect phosphatidylserine (PS) exposure and membrane permeability by annexin V and 7AAD staining. Four cell populations were observed: annexin^{-}7AAD^{-} (live cells), annexin^{+}7AAD^{-} (early apoptotic), annexin^{+}7AAD^{+} (mid apoptotic or necrotic), and annexin^{-}7AAD^{+} (late apoptotic or necrotic). (A) Shown is the percentage of cell death and the fraction of those cells which are classified as early apoptotic (black bars), mid apoptotic/necrotic (gray bars), and late apoptotic/necrotic (white bars). The means and standard deviations for at three independent experimental replicates are shown (error bars appear

absent when they are smaller than the symbol). *p<0.05, **p<0.01 (two sample t-test), when comparing treated cells to untreated control cells at the indicated time point. (B) Representative flow cytometry plots depicting the time-dependent induction of cell death for TK6 cells treated with 0 μg/ml (untreated) or 0.1 μg/ml (high dose) MNNG. (C) Illustration of apoptotic versus necrotic modes of cell death. Cells that undergo apoptosis move in a counter-clockwise manner, with PS exposure occurring prior to loss of membrane permeability.

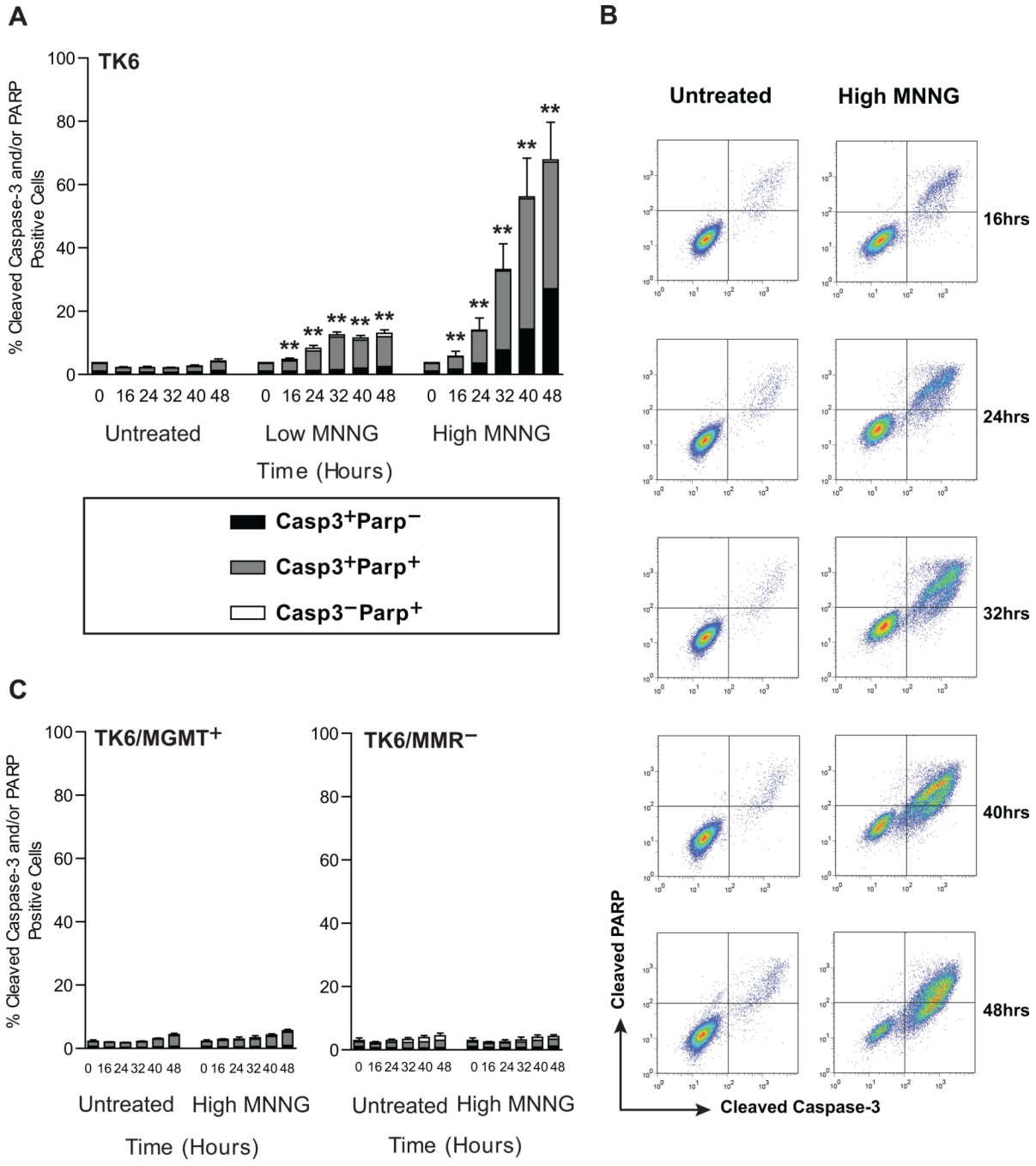

Figure 3. An O^6MeG/MMR-dependent apoptotic cell death is induced in the second cell cycle

Cells undergoing apoptosis were detected by flow cytometry using antibodies against cleaved (active) caspase-3 and cleaved (inactive) PARP. (A) TK6 cells were treated with 0 μg/ml, 0.01 μg/ml (low dose), or 0.1 μg/ml (high dose) MNNG and analyzed at the indicated time points. The figure represents the percentage of apoptosis classified according to cleaved caspase-3 and cleaved PARP levels: cleaved casp3$^+$cleaved parp$^-$ (black bars), cleaved casp3$^+$cleaved parp$^+$ (gray bars), or cleaved casp3$^-$cleaved parp$^+$ (white bars). The means and standard deviations for at least three independent experimental replicates are shown (error bars appear absent when they are smaller than the symbol). *p<0.05, **p<0.01 (two sample t-test), when comparing treated cells to untreated control cells at the indicated time

point. (B) Representative flow cytometry plots of TK6 cells treated with 0 μg/ml (untreated) or 0.1 μg/ml (high dose) MNNG. (C) Percent apoptosis of TK6/MGMT^{+} cells and TK6/MMR^{-} cells after treatment with 0 μg/ml and 0.1 μg/ml MNNG. The means and standard deviations for two or more independent experimental replicates are shown (error bars appear absent when they are smaller than the symbol). *$p<0.05$, **$p<0.01$ (two sample t-test), when comparing treated cells to untreated control cells at the indicated time point.

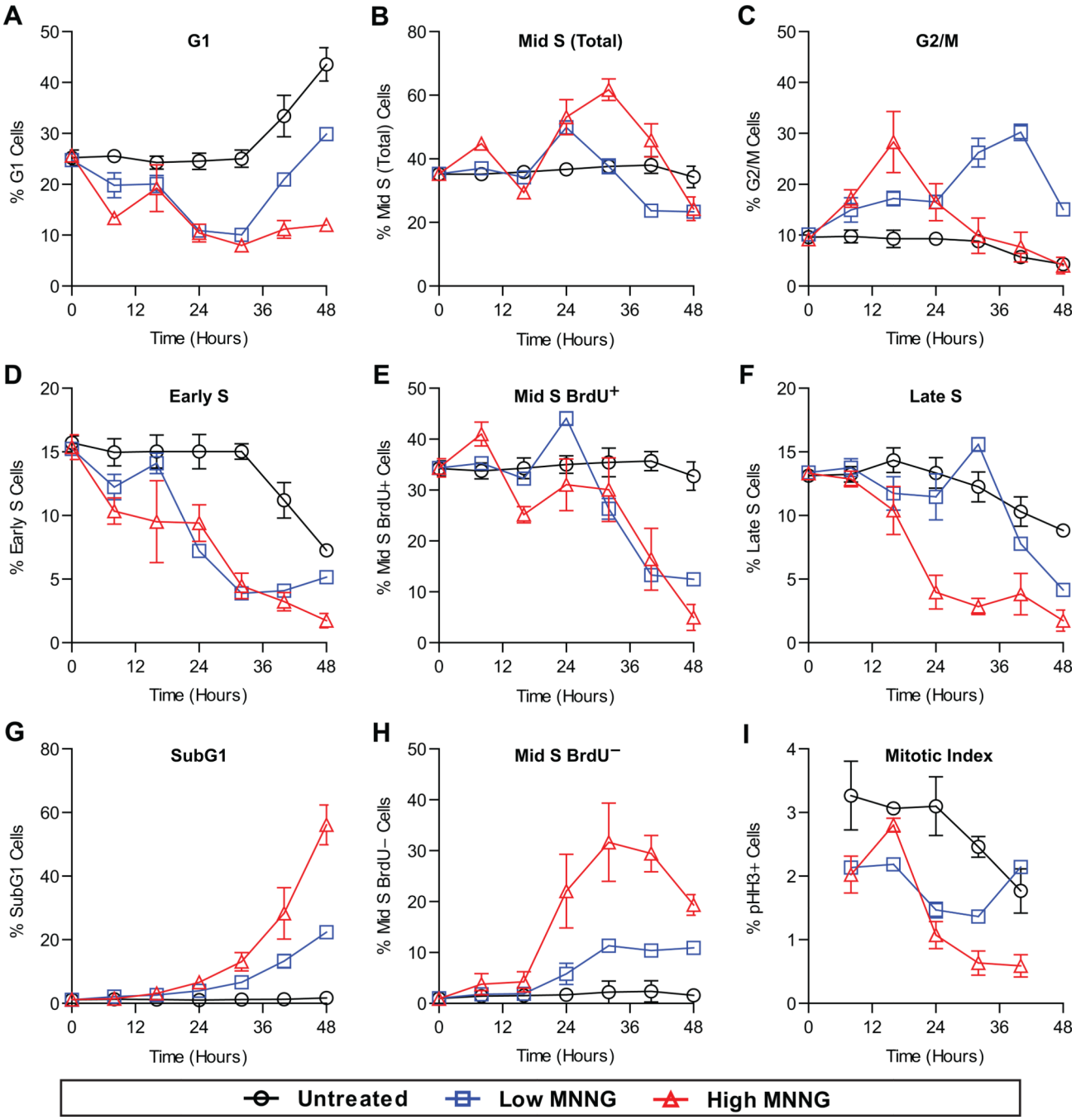

Figure 4. MNNG induces a complex pattern of cell cycle perturbations in TK6 cells with delays in cell cycle progression occurring in both the first and second cell cycle post treatment

(A–H) Cells were pulse labeled with BrdU for one hour prior to the indicated time point and subsequently analyzed both for the incorporation of BrdU into replicating DNA and for total DNA content. Plotted is the percentage of TK6 cells in each phase of the cell cycle following treatment with 0 μg/ml (—○—), 0.01 μg/ml (—□—), or 0.1 μg/ml (—△—) MNNG. (I) Percent of TK6 cells staining positive for the mitotic marker, phospho-histone H3, following treatment with 0 μg/ml (—○—), 0.01 μg/ml (—□—), or 0.1 μg/ml (—△—) MNNG. For all panels, the means and standard deviations for three independent experimental replicates are shown

(error bars appear absent when they are smaller than the symbol). Note that the axes are on different scales to highlight the dynamics of each of the cell cycle stages.

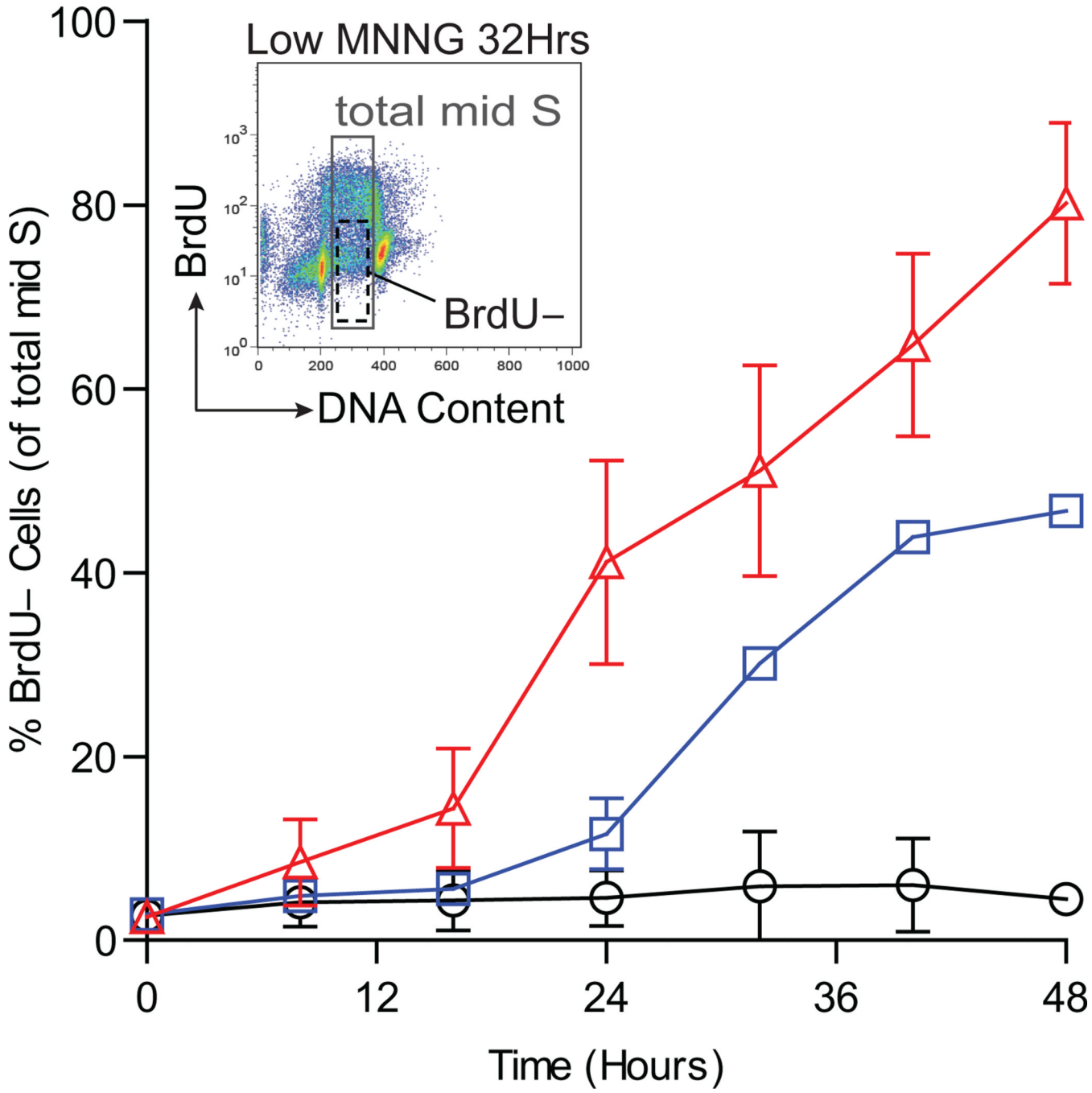

Figure 5. DNA synthesis is inhibited in TK6 cells in the second S-phase following MNNG treatment in a dose-dependent manner

The percent of mid S-phase cells that are negative for BrdU incorporation into replicating DNA following treatment with 0 μg/ml (⊖), 0.01 μg/ml (⊟), or 0.1 μg/ml (△) MNNG is shown. TK6 cells are pulse labeled with BrdU for one hour prior to the indicated time point. The means and standard deviations for three independent experimental replicates are shown (error bars appear absent when they are smaller than the symbol).

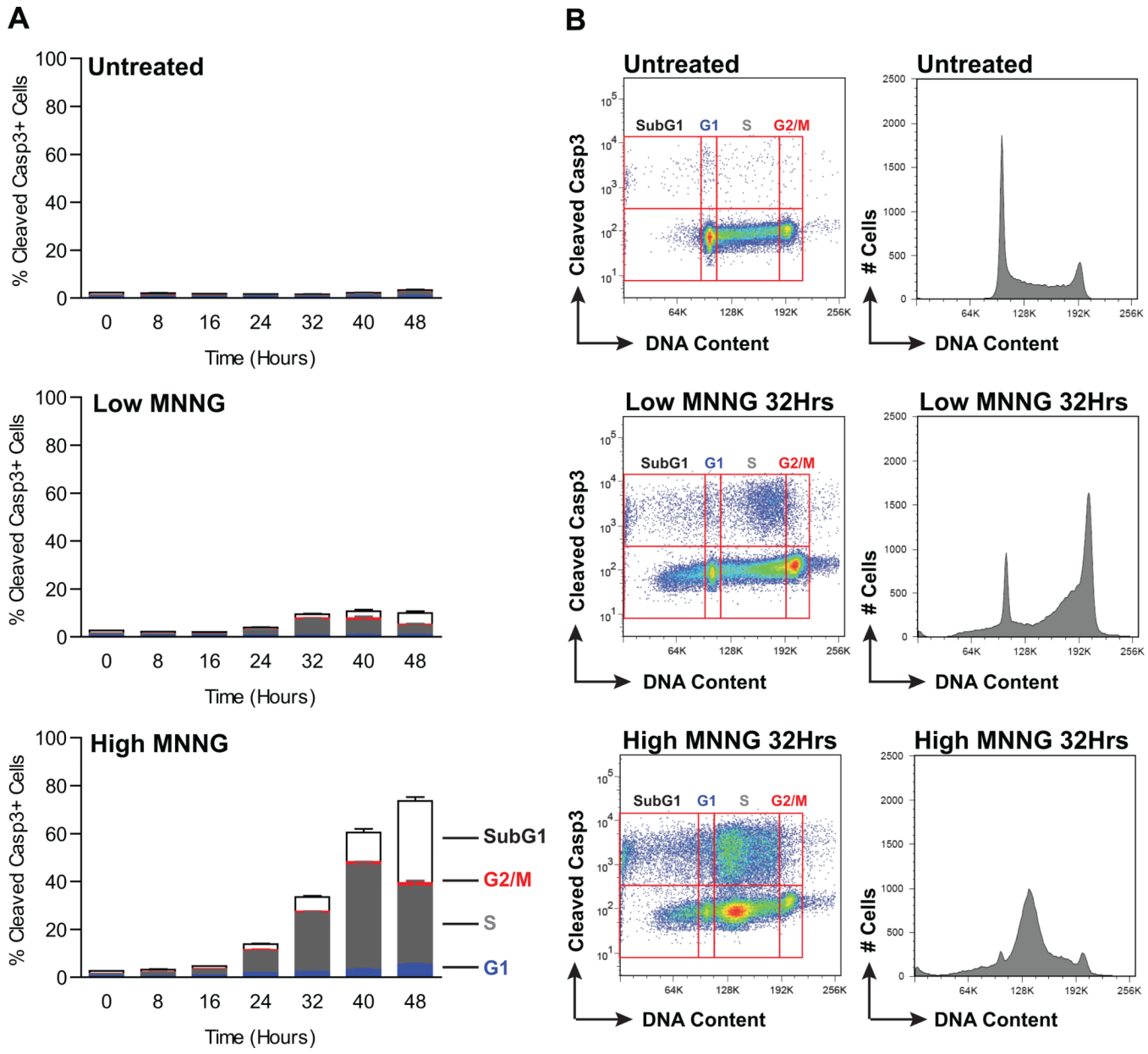

Figure 6. Apoptosis is triggered in the second cell cycle S-phase

TK6 cells were treated with 0 μg/ml (untreated), 0.01 μg/ml (low MNNG), or 0.1 μg/ml (high MNNG) and analyzed for cleaved (active) caspase-3 along with DNA content. (A) Percentage of cleaved caspase-3 cells according to their cell cycle state; G1 (blue), S phase (gray), G2/M (red), and subG1 (white). The means and standard deviations for three independent experimental replicates are shown (error bars appear absent when they are smaller than the symbol). (B) Representative flow cytometry plots of cleaved caspase-3 versus DNA content and the corresponding DNA content histogram 32 hours after treatment with MNNG.

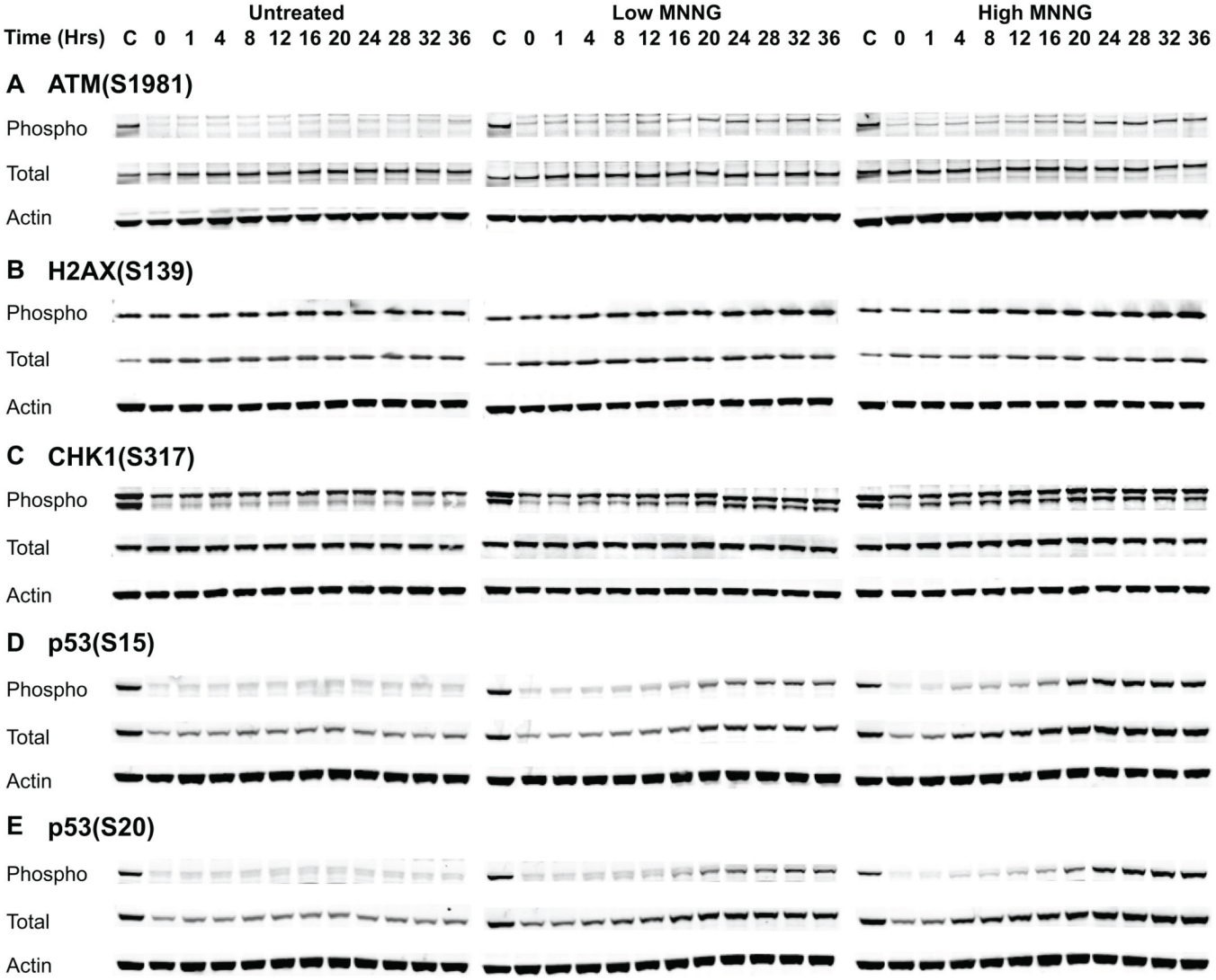

Figure 7. Western blot analysis detects phosphorylation of ATM, H2AX, CHK1, and p53

Extracts were obtained from TK6 cells treated with 0 μg/ml (untreated), 0.01 μg/ml (low MNNG), or 0.1 μg/ml (high MNNG) and immunoblotted with (A) anti-phospho-S1981 ATM and anti-total ATM (B) anti-phospho-S139 H2AX and anti-total H2AX (C) anti-phospho-S317 CHK1 and anti-total CHK1 (D) anti-phospho-S15 p53 and anti-total p53 (E) anti-phospho-S20 p53 and anti-total p53 specific antibodies. Actin was used as a loading control. Positive control lysate (C) was run on each gel to account for experimental variation. For positive controls, TK6 cells were collected 1 hour (ATM, H2AX, and CHK1) or 2 hours (p53) after treatment with 10 Gy IR.

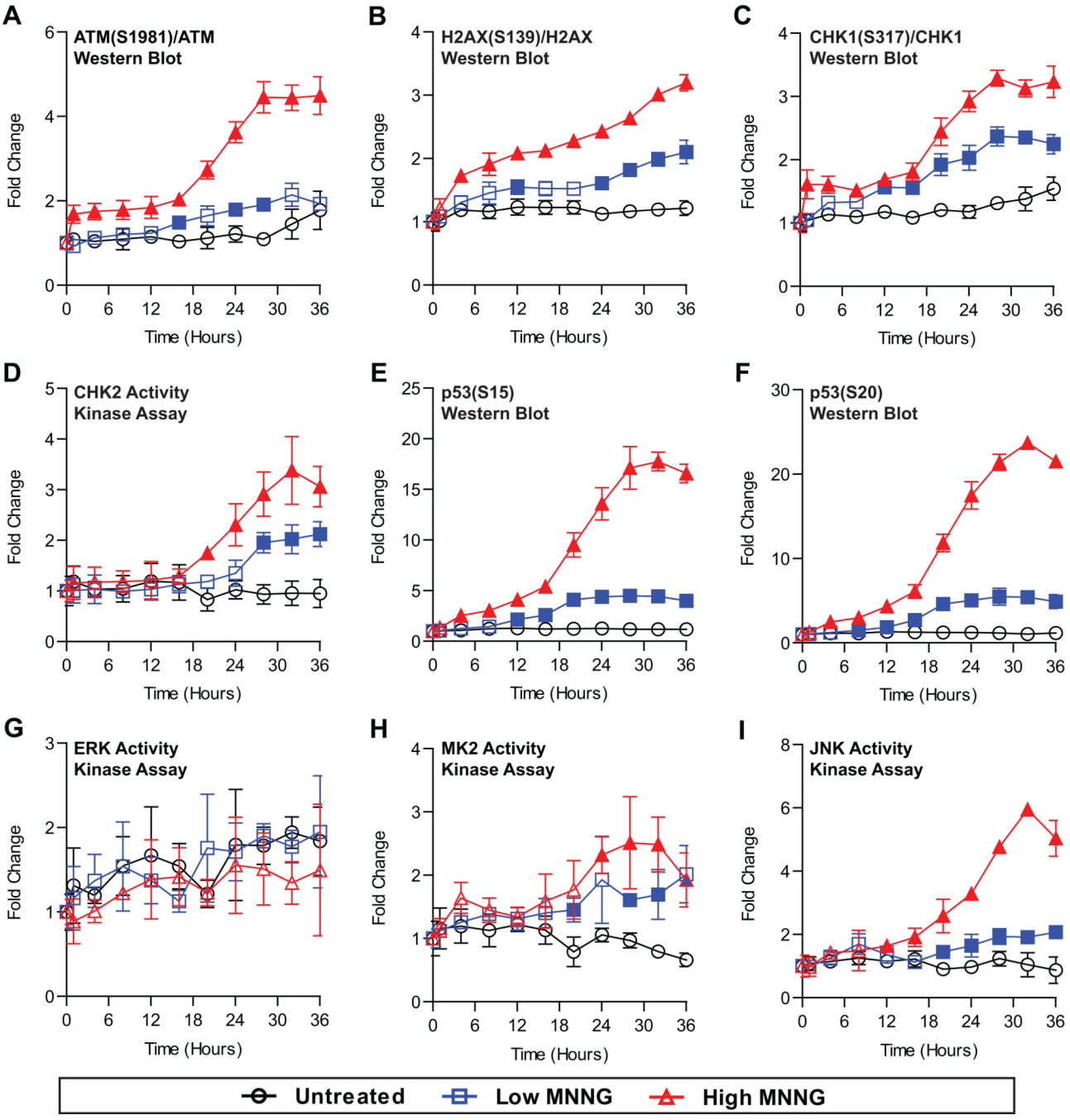

Figure 8. Protein signaling measurements reveal early and late signaling dynamics after TK6 cell treatment with MNNG

Phosphorylation or activation of DNA damage signaling proteins were monitored by western blot or kinase activity assay, respectively, after TK6 cell treatment with 0 μg/ml (—○—), 0.01 μg/ml (—□—), or 0.1 μg/ml (—△—) MNNG. All western blot results were normalized to actin as a loading control. For the indicated proteins, phosphorylation levels were additionally normalized to total levels. Phosphorylation and kinase activity results are plotted as fold change relative to 0 hours. The means and standard deviations for three independent experimental replicates are shown (error bars appear absent when they are

smaller than the symbol). Filled symbols represent a significant difference between treated and untreated values at the indicated time point (p-value<0.05, two sample t-test).

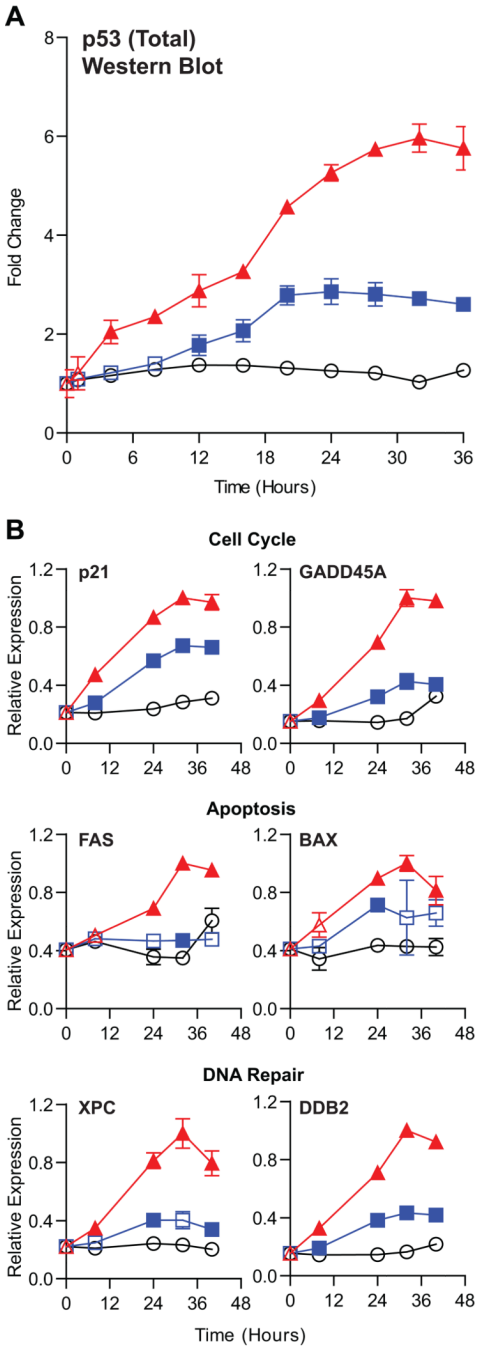

Figure 9. MNNG induces p53 stabilization and activation of downstream p53 transcriptional targets

(A) Total p53 levels were monitored by western blot after TK6 cell treatment with 0 μg/ml (⊖), 0.01 μg/ml (⊟), or 0.1 μg/ml (△) MNNG. Total p53 levels were normalized to actin as a loading control and plotted as fold change relative to 0 hours. The means and standard deviations for three independent experimental replicates are shown (error bars appear absent when they are smaller than the symbol). Filled symbols represent a significant difference between treated and untreated values at the indicated time point (p-value<0.05, two sample t-test). (B) Microarray expression values of known p53 target genes following TK6 cell treatment with 0 μg/ml (⊖), 0.01 μg/ml (⊟), or 0.1 μg/ml (△) MNNG.

Results are normalized to the maximum expression value among all treatments. The means and standard deviations for two independent experimental replicates are shown (error bars appear absent when they are smaller than the symbol). Filled symbols represent a significant difference between treated and untreated values at the indicated time point (p-value<0.05, two sample t-test).

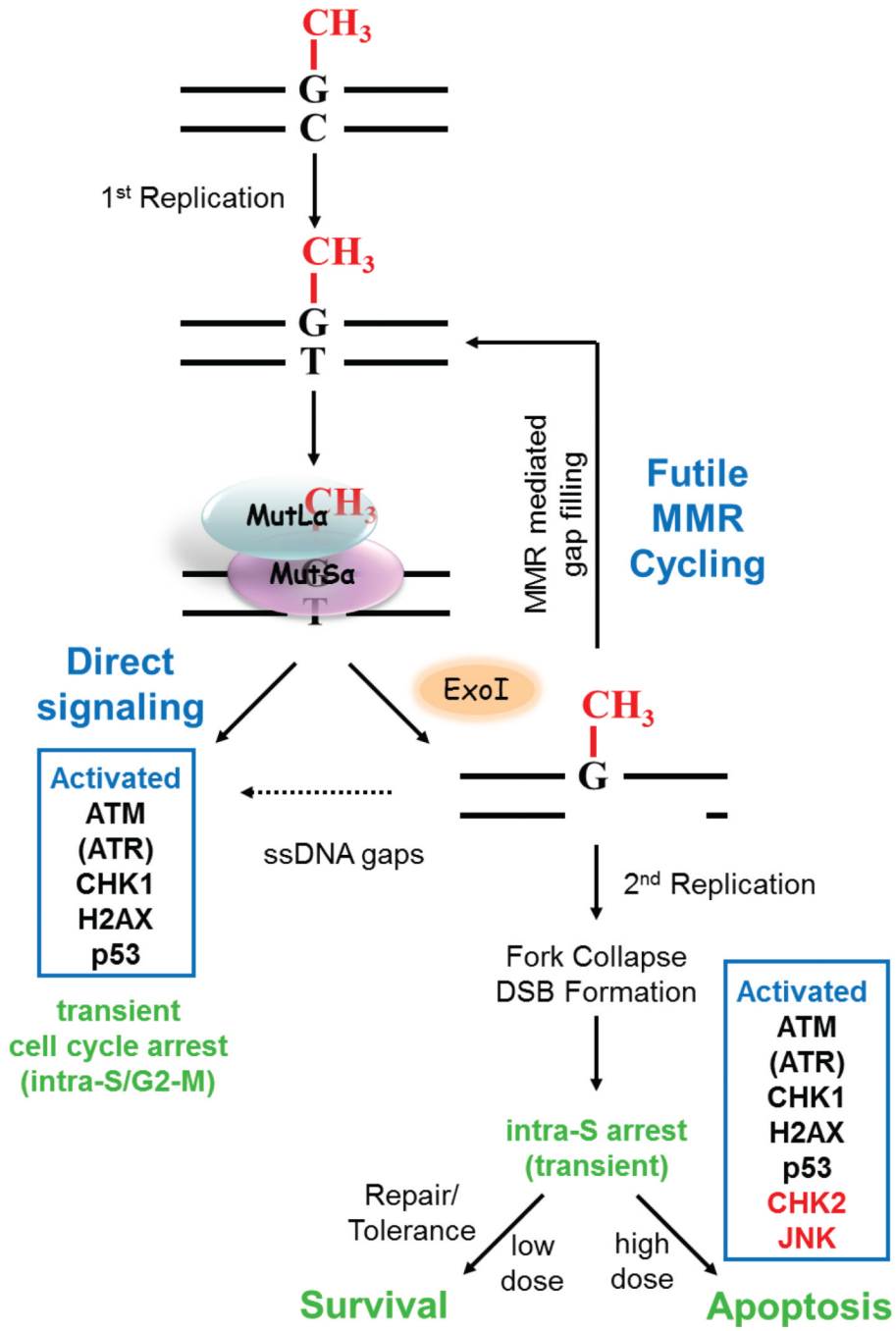

Figure 10. Proposed model for O^6MeG/MMR-dependent cell cycle arrest and cell death

O^6MeG lesions are converted to O^6MeG/T mispairs in the first replication cycle. Subsequently, members of the MMR pathway, MutSα and MutLα, bind to the O^6MeG /T mismatch leading to direct activation of various DDR network proteins and, consequently, the activation of a transient cell cycle arrest in the first cell cycle. In parallel, single-strand DNA (ssDNA) gaps arise due to futile repair attempts by the MMR pathway. The formation of these ssDNA gaps is an additional source of (indirect) signal activation in the first cell cycle. These gaps persist into the second cell cycle where they are encountered by replication forks in the second S-phase. Ultimately, this gives rise to stalled replication forks, fork collapse, and DSB formation. Such events in turn trigger activation of a second

wave of DNA damage signaling. At this time we observe an intra-S-phase arrest. Under low dose conditions, cells are able to repair/tolerate the damage and proceed successfully through the cell cycle. Under high dose conditions, damage ultimately leads to apoptotic cell death out of the second S-phase. Proteins that are regulated in the early- and late-phase are indicated accordingly. While the majority of proteins are regulated in both the first and second cell cycle following MNNG damage, CHK2 and JNK kinase activation occur only after cells proceed into their second cell cycle post treatment. The regulation of ATR is not monitored directly and therefore appears in parentheses.